NASA TECHNICAL NOTE

NASA TN D-6283

A TIME-DEPENDENT METHOD FOR CALCULATING SUPERSONIC ANGLE-OF-ATTACK FLOW ABOUT AXISYMMETRIC BLUNT BODIES WITH SHARP SHOULDERS AND SMOOTH NONAXISYMMETRIC BLUNT BODIES

by Richard W. Barnwell

Langley Research Center
Hampton, Va. 23365

NATIONAL AERONAUTICS AND SPACE ADMINISTRATION • WASHINGTON, D. C. • AUGUST 1971

1. Report No.	2. Government Accession No.	3. Recipient's Catalog No.
NASA TN D-6283		

4. Title and Subtitle	5. Report Date
A TIME-DEPENDENT METHOD FOR CALCULATING SUPERSONIC ANGLE-OF-ATTACK FLOW ABOUT AXISYMMETRIC BLUNT BODIES WITH SHARP SHOULDERS AND SMOOTH NONAXISYMMETRIC BLUNT BODIES	August 1971
	6. Performing Organization Code

7. Author(s)	8. Performing Organization Report No.
Richard W. Barnwell	L-7593
	10. Work Unit No.
9. Performing Organization Name and Address	136-13-05-01
NASA Langley Research Center Hampton, Va. 23365	11. Contract or Grant No.
	13. Type of Report and Period Covered
12. Sponsoring Agency Name and Address	Technical Note
National Aeronautics and Space Administration Washington, D.C. 20546	14. Sponsoring Agency Code

15. Supplementary Notes

16. Abstract

A time-dependent numerical method for calculating supersonic flow about blunt bodies at large angles of attack is presented. The axisymmetric bodies with sharp shoulders which are treated are constructed with a generator composed of segments of constant curvature. The nonaxisymmetric bodies have continuous slope and curvature. All flow fields are inviscid and adiabatic and have one plane of symmetry.

A modification to the method of characteristics is introduced for use at the shock wave. A two-step finite-difference method of second-order accuracy is used at the body surface and in the region between the shock and body. A new finite-difference technique is introduced for use at sharp sonic shoulders.

Comparisons of the results of the present method with experiment and the results of other methods are made for the flow of equilibrium air past the Apollo command module at the trim angle of attack and for perfect gas flow past a spherical cap and a spherically blunted cone at angle of attack. Both the cap and the blunted cone are terminated with sharp shoulders. Results are presented also for perfect gas flow past a prolate spheroid with its major axis normal to the flow.

17. Key Words (Suggested by Author(s))	18. Distribution Statement
Angle of attack Blunt-body flow fields Sharp shoulders Nonaxisymmetric bodies Supersonic, hypersonic Time-dependent finite-difference method	Unclassified – Unlimited

19. Security Classif. (of this report)	20. Security Classif. (of this page)	21. No. of Pages	22. Price*
Unclassified	Unclassified	73	$3.00

*For sale by the National Technical Information Service, Springfield, Virginia 22151

A TIME-DEPENDENT METHOD FOR CALCULATING SUPERSONIC ANGLE-OF-ATTACK FLOW ABOUT AXISYMMETRIC BLUNT BODIES WITH SHARP SHOULDERS AND SMOOTH NONAXISYMMETRIC BLUNT BODIES

By Richard W. Barnwell
Langley Research Center

SUMMARY

A time-dependent numerical method for calculating supersonic flow about blunt bodies at large angles of attack is presented. The axisymmetric bodies with sharp shoulders which are treated are constructed with a generator composed of segments of constant curvature. The nonaxisymmetric bodies have continuous slope and curvature. All flow fields are inviscid and adiabatic and have one plane of symmetry.

A modification to the method of characteristics is introduced for use at the shock wave. A two-step finite-difference method of second-order accuracy is used at the body surface and in the region between the shock and body. A new finite-difference technique is introduced for use at sharp sonic shoulders.

Comparisons of the results of the present method with experiment and the results of other methods are made for the flow of equilibrium air past the Apollo command module at the trim angle of attack and for perfect gas flow past a spherical cap and a spherically blunted cone at angle of attack. Both the cap and the blunted cone are terminated with sharp shoulders. Results are presented also for perfect gas flow past a prolate spheroid with its major axis normal to the flow.

INTRODUCTION

Time-dependent finite-difference methods provide a means of treating the problem of inviscid supersonic flow past a blunt body as an initial-value problem since the equations for inviscid transient flow are always hyperbolic. Results for steady flow are obtained from the asymptotic solution to the transient problem. One of the major advantages of these methods is that there is no conceptual difficulty in extending them to treat such three-dimensional effects as angle of attack and nonaxisymmetric body geometry. In general, the chief difficulty encountered in making a three-dimensional, rather than a

two-dimensional, time-dependent calculation is the additional time required to perform the computation.

Time-dependent methods for calculating three-dimensional blunt-body flow fields have been developed by Rusanov (ref. 1), Bohachevsky and Mates (ref. 2), Moretti and Bleich (ref. 3), and Xerikos and Anderson (ref. 4). Only the method of reference 1 can be applied to anything but axisymmetric bodies. All the methods except that of Moretti and Bleich produce results of first-order accuracy in the mesh spacings; the method of reference 3 produces answers of second-order accuracy. The method of Bohachevsky and Mates requires a much larger number of grid points than the other methods because the bow shock wave is treated as an internal feature of the flow rather than as a boundary. As a result, a great deal more computer time is required for this method than for the others.

Cohen, Foster, and Dowty (ref. 5) have employed the refined Godunov method of Masson, Taylor, and Foster (ref. 6) to develop an approximate time-dependent method for calculating angle-of-attack flow. The flow is calculated in the plane of symmetry, and trigonometric functions are used to approximate the cross-flow derivatives.

The purpose of this paper is to present a time-dependent method for calculating three-dimensional flow fields about two fairly general classes of bodies. The first class is that of axisymmetric bodies and includes bodies with discontinuous surface slope and curvature. The second class is that of nonaxisymmetric bodies with one plane of symmetry and with continuous surface slope and curvature. Both perfect and equilibrium gas models can be treated. A previous version of this method for calculating flow about axisymmetric bodies with sharp shoulders at angle of attack was presented in reference 7. The present method is a refinement of a previous method presented in references 8 and 9 and extends the applicability of that method to three dimensions. As was the case for the method of references 8 and 9, the present method is closely related to that of Moretti and coauthors (refs. 3 and 10).

SYMBOLS

A,B,C,C',D,E,E',F points in figures 4 and 5

$\tilde{A},\tilde{B},\tilde{C}$ matrices defined by equations (B2)

A_i,B_i,C_i,D_i,E_i quantities defined by equation (6)

a	speed of sound
$\bar{a},\bar{b}$	semimajor and semiminor axes of prolate spheroid
$\bar{B}_i,\bar{D}_i,\bar{E}_i$	quantities defined by equations (15)
$\tilde{D}$	vector defined by equations (B2)
$\tilde{E}$	matrix defined by equation (B11)
e	internal energy
$\tilde{e}$	eigenvalue of matrix $\tilde{E}$
$\bar{e}$	quantity defined by equation (B17)
$\vec{e}_s$	unit vector normal to shock, defined by equation (26)
$\vec{e}_{\overline{V}_\infty}$	unit vector in free-stream direction, defined by equation (31)
$\vec{e}_x,\vec{e}_y,\vec{e}_\varphi$	unit vectors in x-, y-, and φ-directions, respectively
F,F_c,F_o	quantities used in equation (18)
F_ℓ,F_u	lower and upper bounds for inequality (B20)
$\overline{F}_u(\chi,\bar{\epsilon})$	quantity defined by equation (B24)
f	quantity defined by equation (B13)
$\bar{f}_u(\bar{\epsilon})$	maximum value of $\overline{F}_u(\chi,\bar{\epsilon})$ for given value of $\bar{\epsilon}$
G	quantity defined by equation (25)
$\tilde{G}$	matrix defined by equation (B12)
$\tilde{g}$	eigenvalue of matrix $\tilde{G}$
H	total enthalpy

h	static enthalpy
h_t, h_x, h_y, h_φ	direction cosines of bicharacteristic in t,x,y,φ space
K	curvature of reference surface
L_x, L_y, L_φ	wavelength of error solutions in x-, y-, and φ-directions, respectively
M	Mach number
m	quantity defined by equations (B15)
$\tilde{m}$	quantity defined by equations (B22)
P_1, P_3	quantities defined by equations (B22)
p	pressure
p_o	reference pressure, 1 atmosphere (101.3 kN/m^2)
p_t	exact value of stagnation pressure
Q	quantity defined by equation (B23)
R	quantity equal to right side of equation (33) or (35)
r	perpendicular distance from coordinate axis
r_n	nose radius
r_1, r_2, r_3	quantities defined by equations (B8)
s	distance along surface from axis in plane of constant φ
t	time
U,V	components of velocity tangent and normal to shock, respectively

U_x, U_y, U_φ components of U in x-, y-, and φ-directions, respectively

$\tilde{U}$ quantity defined by equations (B15)

u,v,w components of velocity in x-, y-, and φ-directions, respectively

$\bar{u}, \bar{v}$ velocity components shown in figure 5

$\overline{V}$ magnitude of total velocity

$\tilde{v}$ quantity defined by equation (B3)

W vector defined by equations (B2)

X,x distance along generator of reference surface from axis

Y normalized coordinate defined by equations (7)

y coordinate along normals to reference surface

$\tilde{y} = y - y_b$

z coordinate along axis

α angle of attack

$\tilde{\alpha}$ exponent used in equation (B6)

$\alpha_x, \alpha_y, \alpha_\varphi$ quantities defined by equations (30)

$\beta_x, \beta_y, \beta_\varphi$ quantities defined by equations (24)

γ ratio of specific heats

$\tilde{\gamma}$ ratio of static enthalpy to internal energy, h/e

$\Delta\tau, \Delta X, \Delta Y, \Delta\Phi$ mesh spacings for time τ and coordinates X, Y, and Φ

δ	shock layer thickness, function of τ, X, Φ
ϵ	damping coefficient
$\bar{\epsilon} = \frac{\epsilon}{\epsilon_{max}}$	
ζ	distance from corner, $x_{c,min} - x$
η, ξ, ψ	quantities defined by equations (B7)
θ	angle between normal to reference surface and axis
λ	scale factor for x-coordinate defined by equation (3)
μ_1, μ_2, μ_3	quantities defined by equations (B15)
ν	exponent employed in equation (18)
ν_1, ν_2, ν_3	quantities defined by equations (B22)
ρ	density
σ	angle between normal to shock and free-stream direction
τ	time
Φ, φ	azimuthal angle
χ	quantity which varies from 0 to 1
$\overline{\omega}$	small nonnegative number

Subscripts:

b	properties at body
c	properties at shoulder
I	initial solution

max maximum value

min minimum value

s properties at shock

∞ properties in free stream

90^{o} properties for $\varphi = 90^{o}$

Superscripts:

ω exponent between 0 and 1

$*$ conditions when $u = a$ and $v = 0$

$\cdot$ differentiation with respect to t or τ of functions which do not depend on Y

$'$ differentiation with respect to x or X of functions which do not depend on Y

$\hat{}$ differentiation with respect to φ or Φ of functions which do not depend on Y

$\rightarrow$ vector quantity

ANALYSIS

The present method for calculating numerical solutions for time-dependent, inviscid, three-dimensional flow past blunt bodies traveling at supersonic speeds is described in this section. A number of grid points are located on the bow shock wave, the body surface, and between the shock and surface. The region of computation must contain the entire zone of subsonic flow. An initial solution, which can be quite general, is assumed; and the flow at each of the grid points is calculated for a number of time steps. At each cycle of the computation an initial-value problem is solved to determine the solution at the new time step from the solution at the previous time step, subject to the appropriate boundary conditions. Results for steady flow are obtained after many time steps when the time derivatives of the flow properties are sufficiently small. It should be noted that the locations of the grid points adjust with time as the location of the bow shock adjusts.

A two-step finite-difference approximation to the time-dependent method of characteristics is used at the bow shock wave, whereas the two-step, time-dependent, finite-difference scheme of Brailovskaya (ref. 11) is used at the surface and between the shock and surface. The solution for a given time step is determined first at the points on the shock wave, then at those between the shock and body, and finally at those on the body surface.

Both the present method and the method of references 8 and 9 can be used to calculate axisymmetric flow about blunt bodies with sharp sonic shoulders. A major advantage of the present method is that it is not necessary to specify any of the flow properties at the shoulder. With the method of references 8 and 9, it is necessary to specify that the Mach number at the shoulder is 1 when the flow upstream of the shoulder is subsonic. A second advantage of the present method is that the computational techniques which are used at the bow shock wave and body surface are much more efficient than the conventional time-dependent method of characteristics which is used in references 8 and 9.

Basic Coordinate System and Governing Equations

The basic coordinate system which is used is similar to that employed in references 8 and 9. An axisymmetric reference surface is established as shown in figure 1. The coordinates are the azimuthal angle φ and the distances x and y, which are measured along the reference surface and normal to it, respectively, in planes of constant φ. The components of velocity in the x-, y-, and φ-directions are u, v, and w. The angle in a plane of constant φ between the normal to the reference surface and the direction of the coordinate axis is designated as θ and satisfies the differential equation

$$\frac{d\theta}{dx} = K \tag{1}$$

where K is the local curvature of the reference surface. The distance r from the axis is given by the equation

$$r(x,y) = \int_{\bar{x}=0}^{\bar{x}=x} \cos\,\theta(\bar{x})d\bar{x} + y \sin\,\theta(x)$$

As stated previously, the bodies which the present method will treat have one plane of symmetry. The free-stream velocity vector is parallel to this plane. The angle φ is measured from the leeward side of this plane, and the reference surface is constructed of segments of constant curvature. The reference surface shown in figure 1 is constructed of one segment and hence is spherical.

The type of coordinate system to be used with an axisymmetric body with a sharp shoulder is shown in figure 2. The reference surface which is used with the body in the

figure has three segments of constant curvature. The coordinate system is focused at the corner in the manner of references 8 and 9 so that in the vicinity of the shoulder $\left(x_{c,min} \leqq x \leqq x_{c,max}\right)$ the line of intersection of the reference surface and a plane of constant φ is a circular arc centered at the shoulder. The use of a coordinate system which focuses at sharp shoulders is crucial to the present method.

The coordinate system to be used with an axisymmetric body without sharp shoulders but with a generator composed of segments of constant curvature is similar to that used with bodies with sharp shoulders in that the reference surface is located at a constant distance y_b from the body along the normals to these surfaces. For nonaxisymmetric bodies, the distance y_b is generally a function of x and φ.

The equations for the conservation of mass and momentum, written in dimensional form in terms of the time t and the coordinates x, y, and φ, are

Continuity:

$$\frac{d\rho}{dt} + \rho\left[\frac{1}{\lambda}\frac{\partial u}{\partial x} + \frac{\partial v}{\partial y} + \frac{1}{r}\frac{\partial w}{\partial \varphi} + \frac{\cos\theta}{r}u + \left(\frac{K}{\lambda} + \frac{\sin\theta}{r}\right)v\right] = 0 \tag{2a}$$

x-momentum:

$$\frac{du}{dt} + \frac{1}{\lambda\rho}\frac{\partial p}{\partial x} + \frac{K}{\lambda}uv - \frac{\cos\theta}{r}w^2 = 0 \tag{2b}$$

y-momentum:

$$\frac{dv}{dt} + \frac{1}{\rho}\frac{\partial p}{\partial y} - \frac{K}{\lambda}u^2 - \frac{\sin\theta}{r}w^2 = 0 \tag{2c}$$

φ-momentum:

$$\frac{dw}{dt} + \frac{1}{\rho r}\frac{\partial p}{\partial \varphi} + \frac{\cos\theta}{r}uw + \frac{\sin\theta}{r}vw = 0 \tag{2d}$$

where p and ρ are the pressure and density of the gas, λ is the scale factor for the x-coordinate and satisfies the equation

$$\lambda = 1 + yK \tag{3}$$

and d/dt is the total derivative with respect to time along a streamline and can be written as

$$\frac{d}{dt} = \frac{\partial}{\partial t} + \frac{u}{\lambda}\frac{\partial}{\partial x} + v\frac{\partial}{\partial y} + \frac{w}{r}\frac{\partial}{\partial \varphi}$$

In this paper, the energy equation is used in the forms

$$\frac{de}{dt} - \frac{p}{\rho^2}\frac{d\rho}{dt} = 0 \tag{4a}$$

and

$$\frac{dp}{dt} + a^2\rho\left[\frac{1}{\lambda}\frac{\partial u}{\partial x} + \frac{\partial v}{\partial y} + \frac{1}{r}\frac{\partial w}{\partial \varphi} + \frac{\cos\theta}{r}u + \left(\frac{K}{\lambda} + \frac{\sin\theta}{r}\right)v\right] = 0 \tag{4b}$$

where e and a are the internal energy and speed of sound of the gas, respectively.

It should be noted that equations (2) and (4a) can be written in conservation form as

$$\frac{\partial A_i}{\partial t} + \frac{\partial B_i}{\partial x} + \frac{\partial C_i}{\partial y} + \frac{\partial D_i}{\partial \varphi} + E_i = 0 \qquad (i = 1,2,3,4,5) \tag{5}$$

where

$$\left.\begin{array}{llll}
A_1 = \rho\lambda & B_1 = \rho u & C_1 = \rho v\lambda & D_1 = \rho w\frac{\lambda}{r} \\
A_2 = \rho u\lambda & B_2 = p + \rho u^2 & C_2 = \rho uv\lambda & D_2 = \rho uw\frac{\lambda}{r} \\
A_3 = \rho v\lambda & B_3 = \rho uv & C_3 = (p + \rho v^2)\lambda & D_3\ \rho vw\frac{\lambda}{r} \\
A_4 = \rho w\lambda & B_4 = \rho uw & C_4 = \rho vw\lambda & D_4 = (p + \rho w^2)\frac{\lambda}{r} \\
A_5 = (\rho H - p)\lambda & B_5 = \rho uH & C_5 = \rho vH\lambda & D_5 = \rho wH\frac{\lambda}{r}
\end{array}\right\} \tag{6}$$

$$E_1 = (\rho u\cos\theta + \rho v\sin\theta)\frac{\lambda}{r}$$

$$E_2 = \rho(u^2 - w^2)\frac{\lambda}{r}\cos\theta + \rho uv\left(K + \frac{\lambda}{r}\sin\theta\right)$$

$$E_3 = \rho uv\frac{\lambda}{r}\cos\theta + \rho(v^2 - w^2)\frac{\lambda}{r}\sin\theta - K(p + \rho u^2)$$

$$E_4 = 2(\rho uw\cos\theta + \rho vw\sin\theta)\frac{\lambda}{r}$$

$$E_5 = (\rho uH\cos\theta + \rho vH\sin\theta)\frac{\lambda}{r}$$

The quantity H in equations (6) is the total enthalpy and is written as

$$H = h + \frac{1}{2}\left(u^2 + v^2 + w^2\right)$$

where h is the static enthalpy of the gas.

Computational Coordinates

The shock-wave and body-surface locations are specified by the equations

$$y = y_s(t,x,\varphi)$$

and

$$y = y_b(x,\varphi)$$

respectively, and the distance between the shock and surface for given values of t, x, and φ is $\delta = y_s - y_b$. The function y_b for the body surface is known, and the functions y_s and δ must be determined as part of the solution.

In this paper, calculations are made in terms of the independent variables

$$\tau = t \qquad X = x \qquad Y = \frac{y - y_b}{\delta} \qquad \Phi = \varphi \tag{7}$$

It should be noted that the geometrical variables X, Y, and Φ do not form an orthogonal set. The partial derivatives with respect to t, x, y, and φ are related to those with respect to τ, X, Y, and Φ as follows:

$$\left.\begin{aligned}
\frac{\partial}{\partial t} &= \frac{\partial}{\partial \tau} - \frac{Y\dot{\delta}}{\delta}\frac{\partial}{\partial Y} \\
\frac{\partial}{\partial x} &= \frac{\partial}{\partial X} - \frac{1}{\delta}\left(Y\delta' + y_b'\right)\frac{\partial}{\partial Y} \\
\frac{\partial}{\partial y} &= \frac{1}{\delta}\frac{\partial}{\partial Y} \\
\frac{\partial}{\partial \varphi} &= \frac{\partial}{\partial \Phi} - \frac{1}{\delta}\left(Y\hat{\delta} + \hat{y}_b\right)\frac{\partial}{\partial Y}
\end{aligned}\right\} \tag{8}$$

where $\dot{\delta}$, δ', and $\hat{\delta}$ are the derivatives of δ with respect to τ, X, and Φ, respectively.

The shock layer to be calculated is subdivided with the X-, Y-, and Φ-coordinate surfaces as shown in figure 3. The planes of constant Φ are spaced from $\Phi = 0^{o}$ to $\Phi = 180^{o}$ with a uniform mesh spacing $\Delta\Phi$. Since the flow fields which are treated in this paper have one plane of symmetry, only one side needs to be calculated. The coordinate Y has values of 0 and 1 at the body and shock, respectively. A uniform mesh spacing ΔY separates the surfaces of constant Y which are located between the surface and shock wave. The coordinate X is measured along the generator of the axisymmetric reference surface. As stated previously, this generator is constructed of segments of constant curvature (the generator illustrated in fig. 3 has two such segments). The surfaces of constant X are spaced so that the distance separating them along the generator of the reference surface is a constant spacing ΔX. It should be noted that the surfaces of constant X are orthogonal to the reference surface.

The flow properties are calculated at the intersections of the surfaces of constant X, Y, and Φ. Since the Y-coordinate is normalized with respect to the distance between the shock wave and the body surface, the locations of the grid intersections move as the shock wave adjusts to its steady position.

Calculation of Flow Within Shock Layer

The procedure for the calculation of flow within the shock layer is used at the grid points between the shock and surface. A related approach is used at most of the points on the surface.

General procedure.- The equations which are solved are equations (5) in terms of the independent variables τ, X, Y, and Φ and are written as

$$\frac{\partial A_i}{\partial \tau} = -\left\{ \frac{\partial B_i}{\partial X} + \frac{1}{\delta}\frac{\partial}{\partial Y}\left[C_i - Y\dot{\delta}A_i - \left(y_b' + Y\delta'\right)B_i - \left(\hat{y}_b + Y\hat{\delta}\right)D_i \right] + \frac{\partial D_i}{\partial \Phi} + E_i + \frac{1}{\delta}\left(\dot{\delta}A_i + \delta' B_i + \hat{\delta}D_i\right) \right\} \qquad (i = 1,2,3,4,5) \qquad (9)$$

The quantities y_b' and $\hat{y}_b$ are the derivatives of y_b with respect to X and Φ, respectively.

The equations are used in this particular conservation form because the conserved functions have continuous derivatives in the vicinity of sharp sonic shoulders although some of the flow properties have unbounded derivatives at these shoulders. The advantages of using this form to obtain solutions on streamlines near sharp shoulders were discussed in reference 9, and the advantages of using it on surface streamlines are discussed subsequently.

As stated in reference 9, the derivatives with respect to Y in equations (9) are well behaved at points in the flow field near sharp shoulders because the quantities which are differentiated are proportional to Y at these shoulders. This follows because the segment of the generator of the reference surface associated with the shoulder is a circular arc with its origin at the shoulder as shown in figure 2. Hence, y_b is constant at the shoulder so that

$$y_b' = 0 \qquad \hat{y}_b = 0 \qquad X_{c,min} \leqq X \leqq X_{c,max}$$

The scale factor λ at points near the shoulder satisfies the equation

$$\lambda = \frac{\delta}{|y_b|} Y$$

Note that the quantity y_b is always negative for a sharp shoulder. Since the quantities C_i are all proportional to λ, it follows that these terms are proportional to Y near the shoulder. In view of these considerations, the quantities which are differentiated with respect to Y in equations (9) satisfy the following relationship near sharp shoulders:

$$C_i - Y\dot{\delta}A_i - \left(Y\delta' + y_b'\right)B_i - \left(Y\hat{\delta} + \hat{y}_b\right)D_i = C_i - Y\left(\dot{\delta}A_i + \delta'B_i + \hat{\delta}D_i\right) \propto Y$$

A two-step, time-dependent, finite-difference method of second-order accuracy in the mesh spacings ΔX, ΔY, and $\Delta\Phi$ and first-order accuracy in $\Delta\tau$ is used to integrate the governing equations. This method was first used by Brailovskaya (ref. 11). In the first step the time derivative is approximated with a forward-difference expression, whereas in the second step the time derivative is replaced with a backward-difference expression. The first-step solution, which is designated with the subscript I, is determined with the equations

$$A_{i,I}(\tau,X,Y,\Phi) = A_i(\tau-\Delta\tau,X,Y,\Phi) + \Delta\tau \frac{\partial}{\partial\tau} A_i(\tau-\Delta\tau,X,Y,\Phi) \qquad (i = 1,2,3,4,5) \qquad (10)$$

The partial derivatives $\partial A_i/\partial\tau$ in equations (10) are determined by evaluating the right side of equations (9) at the point $(\tau - \Delta\tau,X,Y,\Phi)$. Unless otherwise noted, the partial derivatives with respect to X, Y, and Φ in equations (9) are approximated with central-difference formulas. For example, the partial derivatives $\partial B_i/\partial X$ in equations (9) are approximated with the expressions

$$\frac{\partial}{\partial X} B_i(\tau-\Delta\tau,X,Y,\Phi) = \frac{1}{2\,\Delta X}\left[B_i(\tau-\Delta\tau,X+\Delta X,Y,\Phi) - B_i(\tau-\Delta\tau,X-\Delta X,Y,\Phi)\right]$$

The second-step solution is obtained with the equations

$$A_i(\tau,X,Y,\Phi) = A_i(\tau-\Delta\tau,X,Y,\Phi) + \Delta\tau \frac{\partial}{\partial\tau} A_{i,I}(\tau,X,Y,\Phi) - \epsilon \left\{(\Delta X)^4 \frac{\partial^4}{\partial X^4} A_i(\tau-\Delta\tau,X,Y,\Phi)\right.$$

$$\left. + (\Delta Y)^4 \frac{\partial^4}{\partial Y^4} A_i(\tau-\Delta\tau,X,Y,\Phi) + (\Delta\Phi)^4 \frac{\partial^4}{\partial\Phi^4} A_i(\tau-\Delta\tau,X,Y,\Phi)\right\}$$

$$(i = 1,2,3,4,5) \qquad (11)$$

where the values of the partial derivatives $\partial A_{i,I}/\partial\tau$ at the point (τ,X,Y,Φ) are determined by evaluating the right side of equations (9) at this point with the first-step solution. The terms of fourth order in equations (11) are nonphysical damping functions similar to that used by Richtmyer and Morton (ref. 12) which are added to eliminate instabilities. Values for these derivatives are determined with five-point formulas of the form

$$(\Delta X)^4 \frac{\partial^4}{\partial X^4} A_i(\tau-\Delta\tau,X,Y,\Phi) = A_i(\tau-\Delta\tau,X+2\Delta X,Y,\Phi) + A_i(\tau-\Delta\tau,X-2\Delta X,Y,\Phi)$$

$$- 4\left[A_i(\tau-\Delta\tau,X+\Delta X,Y,\Phi) + A_i(\tau-\Delta\tau,X-\Delta X,Y,\Phi)\right]$$

$$+ 6A_i(\tau-\Delta\tau,X,Y,\Phi)$$

Five-point formulas of this type cannot be used to evaluate the terms $(\Delta Y)^4 \frac{\partial^4 A_i}{\partial Y^4}$ on surfaces of constant Y adjacent to the shock wave and body surface because points with the coordinates $Y + 2\,\Delta Y$ would be beyond the shock and those with coordinates $Y - 2\,\Delta Y$ would be inside the body. On the surfaces of constant Y next to the shock wave and body surface, the terms $(\Delta Y)^4 \frac{\partial^4 A_i}{\partial Y^4}$ are replaced with terms of the form

$-(\Delta Y)^3 \frac{\partial^3 A_i}{\partial Y^3}$ and $(\Delta Y)^3 \frac{\partial^3 A_i}{\partial Y^3}$, respectively. These quantities are evaluated with the following four-point formulas:

$$\pm(\Delta Y)^3 \frac{\partial^3 A_i}{\partial Y^3} = A_i(\tau-\Delta\tau,X,Y\pm 2\Delta Y,\Phi) - A_i(\tau-\Delta\tau,X,Y\mp\Delta Y,\Phi) - 3\left[A_i(\tau-\Delta\tau,X,Y\pm\Delta Y,\Phi) - A_i(\tau-\Delta\tau,X,Y,\Phi)\right]$$

The density and the velocity components are determined from the quantities A_1, A_2, A_3, and A_4 with the equations

$$\rho = \frac{A_i}{\lambda} \qquad u = \frac{A_2}{A_1} \qquad v = \frac{A_3}{A_1} \qquad w = \frac{A_4}{A_1}$$

The value of the scale factor λ at time τ, which is needed in order to determine the density, is calculated with the following equation obtained by substituting the third of equations (7) into equation (3):

$$\lambda = 1 + \left(\delta Y + y_b\right)K$$

Since it is necessary to know the shock layer thickness δ at time τ, the solution at the shock is determined first at each time step. The internal energy of the gas is determined with the equation

$$e = \frac{A_5}{A_1} - \frac{1}{2}\left(u^2 + v^2 + w^2\right)$$

and the pressure is obtained from the thermodynamic relation

$$p = \rho e(\tilde{\gamma} - 1) \tag{12}$$

where $\tilde{\gamma}$ is the ratio of static enthalpy h to internal energy e ($\tilde{\gamma} = h/e$) with the heat of formation of the gas adjusted so that $h = e = 0$ at a temperature of absolute zero. It should be noted that equation (12) is an exact relation that holds for any gas and is discussed in reference 13. Also, it is shown in that reference that the speed of sound for an equilibrium gas is related to e and $\tilde{\gamma}(\rho,e)$ by the equation

$$a^2 = e\left\{(\tilde{\gamma} - 1)\left[\tilde{\gamma} + \left(\frac{\partial \tilde{\gamma}}{\partial \log_e e}\right)_\rho\right] + \left(\frac{\partial \tilde{\gamma}}{\partial \log_e \rho}\right)_e\right\} \tag{13}$$

For a calorically perfect gas, $\tilde{\gamma}$ is equal to the ratio of specific heats, but these quantities differ for real gases. A curve fit for the thermodynamic function $\tilde{\gamma}$ for equilibrium air in terms of the density ρ and internal energy e is given in reference 13 and is also presented in appendix A. Expressions for the partial derivatives of $\tilde{\gamma}$ in equation (13) are obtained by differentiating the expressions for $\tilde{\gamma}$ given in this appendix.

The Von Neumann conditions provide a means of estimating the permissible values of $\Delta\tau$ and ϵ which can be used at a given time step. It is shown in appendix B that the damping coefficient ϵ must satisfy the inequalities

$$0 \leqq \epsilon \leqq \epsilon_{max} = \frac{1}{24}$$

and that the time step $\Delta\tau$ must satisfy the inequality

$$\Delta\tau \leqq \frac{\bar{f}_u(\bar{\epsilon})\ \min(\lambda\ \Delta X, \delta\ \Delta Y, r\ \Delta\Phi)}{\sqrt{3}\left(\overline{V} + a\right)\sqrt{1 + \frac{1}{2}Q\left(Q + \sqrt{4 + Q^2}\right)}} \tag{14}$$

at each point, where $\overline{V}$ is the magnitude of the total velocity, $\bar{\epsilon} = \epsilon/\epsilon_{max}$, $\bar{f}_u(\bar{\epsilon})$ is a function which is derived and discussed in appendix B, and Q is given by the equation (B23). For each time cycle, the value of $\Delta\tau$ is taken to be the smallest value of the right side of inequality (14) which occurs at any point in the flow field at the previous time step.

Procedure at axis of coordinate system.- The governing partial differential equations (9) contain indeterminate forms on the axis of symmetry, and the velocity components u and w are multivalued with respect to the angle Φ there. In this paper, the solution for $X = 0$ and $\Phi = 0$ is determined with finite-difference equations, and the solution at the axis for Φ not zero is determined algebraically. Indeterminate forms appear in the governing equations at the axis where $X = 0$. When these terms are evaluated with l'Hospital's rule, equations (9) are written as

$$\frac{\partial A_i}{\partial \tau} = -\left\{\frac{\partial \overline{B}_i}{\partial X} + \frac{1}{\delta}\frac{\partial}{\partial Y}\left[C_i - Y\dot{\delta}A_i - \left(y'_b + Y\delta'\right)B_i\right] + \frac{\partial^2 \overline{D}_i}{\partial X\,\partial \Phi} + \overline{E}_i + \frac{1}{\delta}\left(\dot{\delta}A_i + \delta' B_i\right)\right\} \qquad (i = 1,2,3,5)$$

where

$$\left.\begin{aligned}
\overline{B}_i &= 2B_i \qquad (i = 1,3,5) & \overline{E}_1 &= K\rho v \\
\overline{B}_2 &= p + 2\rho u^2 & \overline{E}_2 &= 2K\rho uv \\
\overline{D}_1 &= \rho w & \overline{E}_3 &= -K\left[p + \rho\left(u^2 - v^2\right)\right] \\
\overline{D}_2 &= \rho uw & \overline{E}_5 &= K\rho vH \\
\overline{D}_3 &= \rho vw & & \\
\overline{D}_5 &= \rho wH & &
\end{aligned}\right\} \qquad (15)$$

The cross-flow momentum equation is not needed because it is known from symmetry that $w = 0$ in the plane $\Phi = 0$.

The flow properties for $X = 0$ and $\Phi \neq 0$ are determined from the kinematic relations

$$\left.\begin{aligned}
\rho(\tau,0,Y,\Phi) &= \rho(\tau,0,Y,0) \\
u(\tau,0,Y,\Phi) &= u(\tau,0,Y,0)\cos\Phi \\
v(\tau,0,Y,\Phi) &= v(\tau,0,Y,0) \\
w(\tau,0,Y,\Phi) &= -w(\tau,0,Y,0)\sin\Phi \\
e(\tau,0,Y,\Phi) &= e(\tau,0,Y,0)
\end{aligned}\right\} \qquad (16)$$

Procedure at downstream boundary.- The region of computation terminates at the downstream boundary $X = X_{max}$ where the flow must be supersonic. The procedure which is used at points on this boundary is the same as that used at general points except that the derivatives $\partial B_i/\partial X$ in equations (9) are evaluated with backward differences of the form

$$\frac{\partial}{\partial X} B_i\left(\tau,X_{max},Y,\Phi\right) = \frac{1}{\Delta X}\left[B_i\left(\tau,X_{max},Y,\Phi\right) - B_i\left(\tau,X_{max}-\Delta X,Y,\Phi\right)\right]$$

Procedure where curvature of reference surface is discontinuous.- A special procedure is used for values of X where the curvature of the reference surface changes. As shown in figure 2, these are the locations of the junctions of the segments of constant curvature comprising the generator of the reference surface. The procedure consists of extending the grid on one side of the line of discontinuity or the other by one mesh spacing, as shown in figure 4, and performing the calculation in a mesh block with constant reference-surface curvature. The choice of which grid to extend is determined from the arc lengths along the line $Y = \text{Constant}$ and $\Phi = \text{Constant}$ to the neighboring mesh points; the grid associated with the shortest arc is the one which is used. Thus, the polar grid is used to make calculations for point A since the length of arc AB is less than that of arc AC, and the alternate grid is used at point D since the length of arc ED exceeds that of arc DF.

Calculations are made at points A and D with the appropriate curvature K and equations (9), (10), and (11) as in the general case. Consider point A. The partial derivatives with respect to Y and Φ are formed in the usual manner. The partial derivatives with respect to X at A are determined from the differences between the function B_i at points C' and B. The functions B_i at point C' are determined by interpolating the values at points B and C. The interpolation technique is illustrated in figure 5. First, the components of the velocity in the plane $\Phi = \text{Constant}$ at points B and C are expressed in terms of the components $\bar{u}_B,\bar{v}_B$ and $\bar{u}_C,\bar{v}_C$ which are parallel to the components $u_{C'},v_{C'}$. Then the functions B_i at points B and C are determined in terms of $\bar{u},\bar{v}$ and the other flow properties. Finally, the values of the functions at C' are determined by interpolating between the points B and C. It should be noted that interpolating linearly between points A and C leads to numerical instability.

Calculation of Flow at Body Points With Continuous Slope and Curvature

The procedure which is used at body surface points where the slope and curvature are continuous is similar to that used at points in the shock layer in that calculations are made with equations (9), (10), and (11). The major differences are that the derivatives with respect to Y are evaluated with one-sided second-order finite-difference expressions of the form

$$\frac{\partial}{\partial Y} C_i(\tau,X,0,\Phi) = \frac{1}{2\,\Delta Y}\left[-C_i(\tau,X,2\,\Delta Y,\Phi) + 4C_i(\tau,X,\Delta Y,\Phi) - 3C_i(\tau,X,0,\Phi)\right]$$

and that the damping terms $(\Delta Y)^4 \dfrac{\partial^4 A_i}{\partial Y^4}$ in equations (11) are replaced by terms of the form

$$(\Delta Y)^2 \frac{\partial^2}{\partial Y^2} A_i(\tau-\Delta\tau,X,0,\Phi) = A_i(\tau-\Delta\tau,X,2\Delta Y,\Phi) - 2A_i(\tau-\Delta\tau,X,\Delta Y,\Phi)$$

$$+ A_i(\tau-\Delta\tau,X,0,\Phi)$$

where $Y = 0$ at the surface. At points adjacent to sharp shoulders and at points adjacent to curvature discontinuities where the derivatives of the quantities B_i undergo large changes, the damping terms $(\Delta X)^4 \frac{\partial^4 A_i}{\partial X^4}$ in equations (11) are replaced with terms of the form

$$-(\Delta X)^2 \frac{\partial^2}{\partial X^2} A_i(\tau-\Delta\tau,X,0,\Phi) = -\Big[A_i(\tau-\Delta\tau,X+\Delta X,0,\Phi) - 2A_i(\tau-\Delta\tau,X,0,\Phi)$$

$$+ A_i(\tau-\Delta\tau,X-\Delta X,0,\Phi)\Big]$$

The nature of flow at curvature discontinuities is discussed subsequently. The procedures which are used at the axis of symmetry and the downstream boundary are the same as those used in the shock layer.

Special considerations must be given to the calculation of flow at the surface when there is a discontinuity in either the surface slope or the surface curvature. These considerations are discussed subsequently.

Analysis of Flow at Sharp Shoulder

Consider the flow past an axisymmetric body with a sharp shoulder at angle of attack. At the surface there are two nonzero velocity components, u and w, which are tangent to the surface and in the radial and cross-flow directions, respectively. At the shoulder the u-component is normal to the edge, and the w-component is tangent to it.

Behavior of cross flow at shoulder.- Consider an axisymmetric body with a sharp shoulder such as that shown in figure 2 or 4. It can be shown that the derivative $\partial w/\partial x$ is bounded at a sharp shoulder for steady flow. The steady cross-flow momentum equation is obtained from equation (2d) as

$$\frac{\partial w}{\partial x} = -\frac{1}{r}\left[\frac{1}{u}\left(w \frac{\partial w}{\partial \varphi} + \frac{1}{\rho}\frac{\partial p}{\partial \varphi}\right) + w \cos \theta\right] \tag{17}$$

The quantities w, $1/\rho$, and $1/r$ are known to be finite at the shoulder, and there is no reason for the derivatives with respect to φ to be unbounded. It is shown subsequently that the u-component of velocity must be at least as large as the sonic velocity at the

shoulder so that the quantity $1/u$ is finite. Therefore, it can be concluded that the derivative of w at the shoulder is finite. In this paper it is assumed that this characteristic applies to unsteady as well as steady flow.

Sonic condition for nonzero cross flow.- It is well known that for axisymmetric and plane flow the surface velocity must either be supersonic upon arrival at the shoulder or become sonic there. It can be shown with equations (2) and (4b) that for three-dimensional flow it is the surface component of velocity u, normal to the edge, rather than the total surface velocity $\sqrt{u^2 + w^2}$ which must satisfy one or the other of these conditions. It can be seen from figure 2 that in the vicinity of the shoulder $\left(x_{c,min} \leqq x \leqq x_{c,max}\right)$ the curvature of the reference surface K, the scale factor λ, and the perpendicular distance from the axis r are written as

$$K = \frac{1}{\left|y_b\right|} \qquad \lambda = \frac{\tilde{y}}{\left|y_b\right|} \qquad r = r_c + \tilde{y} \sin \theta$$

respectively, where $\tilde{y} = y - y_b$. By using these relations and equation (1), the equations of motion can be written as

$$\frac{\partial \rho}{\partial t} + \frac{u}{\tilde{y}} \frac{\partial \rho}{\partial \theta} + v \frac{\partial \rho}{\partial \tilde{y}} + \frac{w}{r_c + \tilde{y} \sin \theta} \frac{\partial \rho}{\partial \theta} + \rho \left[\frac{1}{\tilde{y}} \frac{\partial u}{\partial \theta} + \frac{\partial v}{\partial \tilde{y}} + \frac{1}{r_c + \tilde{y} \sin \theta} \frac{\partial w}{\partial \varphi} \right.$$

$$\left. + \frac{\cos \theta}{r_c + \tilde{y} \sin \theta} u + \left(\frac{1}{\tilde{y}} + \frac{\sin \theta}{r_c + \tilde{y} \sin \theta} \right) v \right] = 0$$

$$\frac{\partial u}{\partial t} + \frac{u}{\tilde{y}} \frac{\partial u}{\partial \theta} + v \frac{\partial u}{\partial \tilde{y}} + \frac{w}{r_c + \tilde{y} \sin \theta} \frac{\partial u}{\partial \varphi} + \frac{1}{\rho \tilde{y}} \frac{\partial p}{\partial x} + \frac{uv}{\tilde{y}} - \frac{\cos \theta}{r_c + \tilde{y} \sin \theta} w^2 = 0$$

$$\frac{\partial v}{\partial t} + \frac{u}{\tilde{y}} \frac{\partial v}{\partial \theta} + v \frac{\partial v}{\partial \tilde{y}} + \frac{w}{r_c + \tilde{y} \sin \theta} \frac{\partial v}{\partial \varphi} + \frac{1}{\rho} \frac{\partial p}{\partial \tilde{y}} - \frac{u^2}{\tilde{y}} - \frac{\sin \theta}{r_c + \tilde{y} \sin \theta} w^2 = 0$$

$$\frac{\partial w}{\partial t} + \frac{u}{\tilde{y}} \frac{\partial w}{\partial \theta} + v \frac{\partial w}{\partial \tilde{y}} + \frac{w}{r_c + \tilde{y} \sin \theta} \frac{\partial w}{\partial \varphi} + \frac{1}{\rho \left(r_c + \tilde{y} \sin \theta \right)} \frac{\partial p}{\partial \varphi}$$

$$+ \frac{u \cos \theta + v \sin \theta}{r_c + \tilde{y} \sin \theta} w = 0$$

$$\frac{\partial p}{\partial t} + \frac{u}{\tilde{y}}\frac{\partial p}{\partial \theta} + v\frac{\partial p}{\partial \tilde{y}} + \frac{w}{r_c + \tilde{y}\sin\theta}\frac{\partial p}{\partial \varphi} + a^2\rho\left[\frac{1}{\tilde{y}}\frac{\partial u}{\partial \theta} + \frac{\partial v}{\partial \tilde{y}} + \frac{1}{r_c + \tilde{y}\sin\theta}\frac{\partial w}{\partial \varphi}\right.$$

$$\left. + \frac{\cos\theta}{r_c + \tilde{y}\sin\theta}u + \left(\frac{1}{\tilde{y}} + \frac{\sin\theta}{r_c + \tilde{y}\sin\theta}\right)v\right] = 0$$

Let the flow properties in the vicinity of the corner be represented by functions of the form

$$F(t,\theta,\tilde{y},\varphi) = F_c(t,\theta,\varphi) + \tilde{y}^{\nu(t,\theta,\varphi)}F_o(t,\tilde{y},\theta,\varphi) \tag{18}$$

where F_o is bounded for all values of $\tilde{y}$ and the exponent ν is greater than or equal to zero. When these functions are substituted into the equations of motion, the resulting equations are multiplied by $\tilde{y}$, and the limit is taken as $\tilde{y}$ approaches zero, the terms involving ν and F_o are eliminated, and the following equations are obtained:

$$u_c\frac{\partial \rho_c}{\partial \theta} + \rho_c\left(\frac{\partial u_c}{\partial \theta} + v_c\right) = 0 \tag{19a}$$

$$u_c\left(\frac{\partial u_c}{\partial \theta} + v_c\right) + \frac{1}{\rho_c}\frac{\partial p_c}{\partial \theta} = 0 \tag{19b}$$

$$u_c\left(\frac{\partial v_c}{\partial \theta} - u_c\right) = 0 \tag{19c}$$

$$u_c\frac{\partial w_c}{\partial \theta} = 0 \tag{19d}$$

$$u_c\frac{\partial p_c}{\partial \theta} + a_c^2\rho_c\left(\frac{\partial u_c}{\partial \theta} + v_c\right) = 0 \tag{19e}$$

Equations (19a), (19b), (19c), and (19e) are the Prandtl-Meyer equations where, by assumption, p_c, ρ_c, u_c, v_c, and a_c are functions of t and φ as well as θ. From these equations, it can be shown that the following condition must hold:

$$\frac{\partial \rho_c}{\partial \theta}\left(u_c^2 - a_c^2\right) = 0$$

Thus, the u-component of velocity either must be sonic for $x_{c,min} \leqq x \leqq x_{c,max}$ or it must be supersonic so that the constant-density or wedge-flow solution applies. The solution to equations (19a), (19b), (19c), and (19e) for a perfect gas can be found in appendix B of reference 9. In order to use this solution for angle-of-attack flow fields, the quantity M_C in reference 9 should be interpreted as follows:

$$M_C = \left.\frac{u}{a}\right|_{x=x_{c,min}}$$

Equation (19d) simply states that the cross-flow velocity component is not a function of θ at the shoulder.

Differentials of ρu, $p + \rho u^2$, and ρuH.- Consider isentropic, isoenergetic flow on a surface approaching a sharp shoulder. The differential energy equation can be written as

$$dH = u\,du + w\,dw + dh = 0$$

where

$$dh = \frac{1}{\rho}dp = \frac{a^2}{\rho}d\rho$$

Thus, the differential du can be written as

$$du = -\frac{w}{u}dw - \frac{a^2}{\rho u}d\rho$$

It follows that the differentials of the quantities B_1, B_2, and B_5 can be written as

$$\left.\begin{aligned} d(\rho u) &= \frac{1}{u}\left(u^2 - a^2\right)d\rho - \rho\frac{w}{u}dw \\ d\left(p + \rho u^2\right) &= \left(u^2 - a^2\right)d\rho - 2\rho w\,dw \\ d(\rho uH) &= \frac{H}{u}\left(u^2 - a^2\right)d\rho - \rho\frac{wH}{u}dw \end{aligned}\right\} \tag{20}$$

At a sharp sonic shoulder the quantity $\left(u^2 - a^2\right)d\rho$ in these equations is an indeterminate form and can be evaluated by expanding the thermodynamic properties and the velocity components in terms of the distance from the corner $\zeta = x_{c,min} - x$. It follows from equation (17) that the cross-flow velocity component w varies linearly with ζ. The expressions for the density ρ, the speed of sound a, and the velocity component u are

$$\left.\begin{aligned} \rho &= \rho^* + \rho_1 \zeta^\omega \\ a &= a^* + a_1 \zeta^\omega \\ u &= a^* - u_1 \zeta^\omega \end{aligned}\right\} \tag{21}$$

where ω is a number between 0 and 1 and the coefficients ρ_1, a_1, and u_1 are positive. It has been shown by Guderley (ref. 14) for irrotational flow that ω has a value of 2/5. Friedman (ref. 15) has shown that this value of ω also applies for rotational flow. It can be shown with equations (21) that the indeterminate form can be written to lowest order in ζ as

$$\left(u^2 - a^2\right)d\rho = -2\omega a^* \rho_1 \left(u_1 + a_1\right)\zeta^{2\omega-1}d\zeta$$

Thus, the indeterminate form is, in fact, infinite at the shoulder since the exponent $2\omega - 1$ has a value of -1/5. As a result, the differentials of B_1, B_2, and B_5 in equations (20) are also infinite at the shoulder. Terms of order $3\omega - 1$ and higher do not contribute to the values of the differentials at the shoulder since $3\omega - 1$ has a value of +1/5. It can be seen from equations (21) that the differentials of the thermodynamic properties and the u-component of velocity vary as $\zeta^{\omega-1} = \zeta^{-3/5}$ and, hence, have stronger singularities than the differentials of B_1, B_2, and B_5.

Methods of Calculation at Sharp Shoulders

Two computational procedures are used at sharp shoulders. One procedure is employed when the flow at the shoulder is supersonic and hence nonsingular, and the other is used when the flow is sonic and hence singular. The choice of procedure is made on the basis of the value of the ratio u/a at the previous time step.

Procedure used at sharp supersonic shoulder.- If the u-component of velocity at the shoulder at the previous time step is supersonic, equations (9), (10), and (11) are used as in the general case and the derivatives $\partial B_i/\partial X$ in equations (9) are evaluated with backward-difference expressions. The value of the curvature used in equations (9) is that of the segment of the reference line located upstream of the shoulder. Thus, only the body geometry and the flow upstream of the shoulder influence the solution at the shoulder, as should be the case for supersonic flow. The damping terms $(\Delta X)^4 \dfrac{\partial^4 A_i}{\partial X^4}$ in equations (11) are replaced with second-order terms of the form

$$(\Delta X)^2 \frac{\partial^2}{\partial X^2} A_i(\tau-\Delta\tau,X,0,\Phi) = A_i(\tau-\Delta\tau,X-2\Delta X,0,\Phi) - 2A_i(\tau-\Delta\tau,X-\Delta X,0,\Phi)$$

$$+ A_i(\tau-\Delta\tau,X,0,\Phi) \tag{22}$$

Procedure used at sharp sonic shoulder.- The procedure described for use at a sharp supersonic shoulder was tried also at a sharp sonic shoulder. As is shown in the section on "Results and Discussion," the solution obtained at the shoulder in this manner is subsonic and does not exhibit singular behavior. It is apparent that special consideration must be given to the calculation of flow at a sharp sonic shoulder.

The difficulty with using equations (9) for $i = 1$, 2, and 5 at a sharp sonic shoulder may be due to the fact that each of these equations has two derivatives which become unbounded as a sharp sonic shoulder is approached along the upstream surface in such a manner that the sum of the derivatives is always finite. It has already been shown that the derivatives $\partial B_i/\partial X$ for $i = 1$, 2, and 5 become infinite as a sharp sonic shoulder is approached along the upstream surface. It can be shown that the same behavior is exhibited by the derivatives $\partial C_i/\partial Y$ for $i = 1$, 2, and 5 since the derivative $\partial v/\partial Y$ at the surface becomes infinite as a sonic shoulder is approached from upstream (see ref. 15 for example) and since the scale factor λ does not vanish on the upstream surface. Instead of using equations (9) for $i = 1$, 2, and 5 at sharp sonic shoulders, a set of approximate time-dependent equations are employed.

A set of exact equations in terms of derivatives with respect to X and Φ which is applicable at the body surface for steady flow can be obtained with equations (20), (17), and (8). For example, the first of this set of equations is written as

$$\frac{\partial(\rho u)}{\partial X} - \frac{1}{u}\left(u^2 - a^2\right)\frac{\partial \rho}{\partial X} - \frac{\rho w}{ru}\left[\frac{1}{u}\left(w\frac{\partial w}{\partial \Phi} + \frac{1}{\rho}\frac{\partial p}{\partial \Phi}\right) + w\cos\theta\right] = 0$$

This equation is one form of the steady continuity equation, and the second and third equations in the set are forms of the steady x-momentum and the energy equations, respectively. Therefore, the new equations must be the same as equations (9) for $i = 1$, 2, and 5 in the time-asymptotic limit.

Two basic assumptions are made in order to obtain the approximate time-dependent equations which are used at sonic shoulders in this paper. First, it is assumed that the new set of equations is applicable to transient as well as steady flow when the appropriate time derivatives are added. Second, it is assumed that the terms proportional to the quantity $\left(u^2 - a^2\right)\frac{\partial \rho}{\partial X}$ can be neglected. The approximate time-dependent continuity,

x-momentum, and energy equations which are used at sonic shoulders are written as

$$\left.\begin{aligned}
\frac{\partial(\rho\lambda)}{\partial\tau} &= -\left\{\frac{\partial(\rho u)}{\partial X} - \frac{\rho w}{ru}\left[\frac{1}{u}\left(w\frac{\partial w}{\partial\Phi} + \frac{1}{\rho}\frac{\partial p}{\partial\Phi}\right) + w\cos\theta\right]\right\} \\
\frac{\partial(\rho u\lambda)}{\partial\tau} &= -\left\{\frac{\partial\left(p + \rho u^2\right)}{\partial X} - \frac{2\rho w}{r}\left[\frac{1}{u}\left(w\frac{\partial w}{\partial\Phi} + \frac{1}{\rho}\frac{\partial p}{\partial\Phi}\right) + w\cos\theta\right]\right\} \\
\frac{\partial\left[(\rho H - p)\lambda\right]}{\partial\tau} &= -\left\{\frac{\partial(\rho u H)}{\partial X} - \frac{\rho w H}{ur}\left[\frac{1}{u}\left(w\frac{\partial w}{\partial\Phi} + \frac{1}{\rho}\frac{\partial p}{\partial\Phi}\right) + w\cos\theta\right]\right\}
\end{aligned}\right\} \qquad (23)$$

respectively. The value of the reference-surface curvature K which is used in the expression for λ is that associated with the body surface upstream of the shoulder. The previous version of this method presented in reference 7 differs from the present version in that equation (17) is not used to replace the derivative $\partial w/\partial X$ which otherwise appears in equations (23).

The effect of neglecting the terms proportional to the indeterminate form may be to change the order of the singularity. If the thermodynamic properties and the u-component of velocity near a sonic shoulder vary as $\zeta^{1/2+\overline{\omega}}$ ($\overline{\omega}$ is a small non-negative number) rather than as $\zeta^{2/5}$ as is physically correct, the quantity $\left(u^2 - a^2\right)\frac{\partial\rho}{\partial X}$ would vary as $\zeta^{2\overline{\omega}}$ rather than as $\zeta^{-1/5}$ and hence would vanish at the shoulder.

The numerical procedure which is used at a sharp sonic shoulder consists of integrating equations (23) and the standard cross-flow momentum equation ($i = 4$ in eqs. (9)) with the two-step numerical technique given in equations (10) and (11). The cross-flow momentum equation is used in its standard form since w is not singular at the shoulder. No damping terms are used in the integration of equations (23).

Calculation of Flow at Curvature Discontinuities

Singular behavior can also occur at body points where the curvature of the surface is discontinuous but the slope is continuous. These are the junctions between the segments of constant curvature which compose the generator of the surface. It should be remembered that the only bodies with discontinuities in slope or curvature which are treated with the present method are axisymmetric bodies. Two examples are shown in figure 6. The singular behavior consists of discontinuities in the partial derivatives of p, ρ, and u with respect to X and it can occur for both subsonic and supersonic flow. In general, the streamwise derivatives of the flow properties are discontinuous where the surface curvature is discontinuous. The changes in the derivatives in subsonic regions

where the surface curvature increases abruptly in the direction of flow tend to be much smaller than the changes in the derivatives in supersonic regions and in subsonic regions where the surface curvature decreases abruptly in the direction of flow. It should be noted that the flow tends to compress where the curvature decreases abruptly and it tends to expand where the curvature increases abruptly. The junctions where the X-derivatives tend to undergo large changes are designated by the letter L in figure 6.

If the flow at the junction is supersonic, it is calculated in the same fashion as at a sharp supersonic shoulder. Another procedure is employed when the flow at the junction is subsonic. This procedure involves the use of the governing equations in a form which does not contain curvature terms explicitly. These equations are

$$\frac{\partial \rho}{\partial \tau} + \frac{\partial(\rho u)}{\partial s} + \frac{\rho}{\delta}\frac{\partial v}{\partial Y} + \frac{\partial}{\partial \Phi}\left(\frac{\rho w}{r}\right) + \frac{\cos\theta}{r}\rho u = 0$$

$$\frac{\partial(\rho u)}{\partial \tau} + \frac{\partial\left(p + \rho u^2\right)}{\partial s} + \frac{\rho u}{\delta}\frac{\partial v}{\partial Y} + \frac{\partial}{\partial \Phi}\left(\frac{\rho u w}{r}\right) + \frac{\cos\theta}{r}\rho\left(u^2 - w^2\right) = 0$$

$$\frac{\partial(\rho w)}{\partial \tau} + \frac{\partial(\rho u w)}{\partial s} + \frac{\rho w}{\delta}\frac{\partial v}{\partial Y} + \frac{\partial}{\partial \Phi}\left(\frac{p + \rho w^2}{r}\right) + \frac{2\cos\theta}{r}\rho u w = 0$$

$$\frac{\partial(\rho H - p)}{\partial \tau} + \frac{\partial(\rho u H)}{\partial s} + \frac{\rho H}{\delta}\frac{\partial v}{\partial Y} + \frac{\partial}{\partial \Phi}\left(\frac{\rho w H}{r}\right) + \frac{\cos\theta}{r}\rho u H = 0$$

where s is the distance along the surface from the axis of the coordinate system in a plane of constant Φ so that

$$\frac{\partial}{\partial s} = \frac{1}{\lambda}\frac{\partial}{\partial X}$$

Since the solution at a subsonic junction is influenced by both the upstream and downstream flows, one-sided difference expressions cannot be used to evaluate the derivatives with respect to s. Instead, the upstream and downstream derivatives are evaluated and the results are averaged. Let λ_+ and λ_- be the values of the scale factor for points with values of X greater than and less than that of the junction, respectively. The finite-difference expressions for the partial derivatives with respect to s are

$$\frac{\partial}{\partial s} B_i(\tau,X,0,\Phi) = \frac{1}{2\,\Delta X}\left\{\frac{1}{\lambda_+}\left[B_i(\tau,X+\Delta X,0,\Phi) - B_i(\tau,X,0,\Phi)\right]\right.$$

$$\left. + \frac{1}{\lambda_-}\left[B_i(\tau,X,0,\Phi) - B_i(\tau,X-\Delta X,0,\Phi)\right]\right\} \qquad (i = 1,2,4,5)$$

At points where the modified equations are employed, the damping functions which are used are of the same form as those used at sharp supersonic shoulders and are given by equations (22).

Calculation of Flow at Bow Shock Wave

The method of characteristics is used to determine the flow properties at the bow shock wave. This method consists of solving simultaneously the Rankine-Hugoniot relations for a moving shock and one characteristic compatibility relation. In this paper the characteristic compatibility relation is integrated with a finite-difference technique.

Let the direction cosines of the normal to the shock wave with respect to the x-, y-, and φ-directions at the shock point be $\cos\beta_x$, $\cos\beta_y$, and $\cos\beta_\varphi$, respectively. These quantities can be calculated with the equations

$$\left.\begin{aligned} \cos\beta_x &= -\frac{1}{\lambda G}\frac{\partial y_s}{\partial x} = -\frac{1}{\lambda G}\left(\delta' + y_b'\right) \\ \cos\beta_y &= \frac{1}{G} \\ \cos\beta_\varphi &= -\frac{1}{rG}\frac{\partial y_s}{\partial \varphi} = -\frac{1}{rG}\left(\hat{\delta} + \hat{y}_b\right) \end{aligned}\right\} \qquad (24)$$

where

$$G = \sqrt{\frac{1}{\lambda^2}\left(\delta' + y_b'\right)^2 + \frac{1}{r^2}\left(\hat{\delta} + \hat{y}_b\right)^2 + 1} \qquad (25)$$

The unit vector normal to the shock is written as

$$\vec{e}_s = \vec{e}_x \cos\beta_x + \vec{e}_y \cos\beta_y + \vec{e}_\varphi \cos\beta_\varphi \qquad (26)$$

The Rankine-Hugoniot relations are written in terms of the thermodynamic variables p, ρ, and $\tilde{\gamma} = \frac{h}{e}$, the velocity component normal to the shock V, the component of the shock velocity in the y-direction $\dot{\delta}$, the quantity β_y, the angle σ between the normal to the shock wave and the free-stream direction, and the magnitude of the free-stream velocity $\overline{V}_\infty$ as

$$\left.\begin{aligned} \rho\left(V - \dot{\delta}\sec\beta_y\right) &= \rho_\infty\left(\overline{V}_\infty\cos\sigma - \dot{\delta}\sec\beta_y\right) \\ p + \rho\left(V - \dot{\delta}\sec\beta_y\right)^2 &= p_\infty + \rho_\infty\left(\overline{V}_\infty\cos\sigma - \dot{\delta}\sec\beta_y\right)^2 \\ \frac{\tilde{\gamma}}{\tilde{\gamma}-1}\frac{p}{\rho} + \frac{1}{2}\left(V - \dot{\delta}\sec\beta_y\right)^2 &= \frac{\tilde{\gamma}_\infty}{\tilde{\gamma}_\infty - 1}\frac{p_\infty}{\rho_\infty} + \frac{1}{2}\left(\overline{V}_\infty\cos\sigma - \dot{\delta}\sec\beta_y\right)^2 \end{aligned}\right\} \tag{27}$$

The unsubscripted quantities on the left side of equations (27) are evaluated immediately behind the bow shock wave, whereas the quantities subscripted with ∞ on the right side of these equations are evaluated in the free stream. It should be noted that the normal velocity V is related to the velocity components u, v, and w by the equation

$$V = \vec{e}_S \cdot \vec{\overline{V}} = u\cos\beta_x + v\cos\beta_y + w\cos\beta_\varphi \tag{28}$$

where the total velocity vector $\vec{\overline{V}}$ is expressed as

$$\vec{\overline{V}} = \vec{e}_x u + \vec{e}_y v + \vec{e}_\varphi w \tag{29}$$

Let the direction cosines of the free-stream direction with respect to the x-, y-, and φ-directions of a point be $\cos\alpha_x$, $\cos\alpha_y$, and $\cos\alpha_\varphi$, respectively. Expressions for these quantities are

$$\left.\begin{aligned} \cos\alpha_x &= \sin\theta\cos\alpha + \cos\theta\cos\varphi\sin\alpha \\ \cos\alpha_y &= -\cos\theta\cos\alpha + \sin\theta\cos\varphi\sin\alpha \\ \cos\alpha_\varphi &= -\sin\varphi\sin\alpha \end{aligned}\right\} \tag{30}$$

where α is the angle of attack. The unit vector in the free-stream direction is

$$\vec{e}_{\overline{V}_\infty} = \vec{e}_x\cos\alpha_x + \vec{e}_y\cos\alpha_y + \vec{e}_\varphi\cos\alpha_\varphi \tag{31}$$

The cosine of the angle σ is

$$\cos \sigma = \vec{e}_{\frac{}{V_\infty}} \cdot \vec{e}_S = \cos \alpha_X \cos \beta_X + \cos \alpha_Y \cos \beta_Y + \cos \alpha_\varphi \cos \beta_\varphi \tag{32}$$

The characteristic compatibility relation which is used in this paper is derived in appendix C. It is written in the form

$$\frac{\partial p}{\partial \tau} + \rho a \frac{\partial V}{\partial \tau} = -\left\{\frac{1}{\lambda}\left(u + a \cos \beta_X\right)\frac{\partial p}{\partial X} + \frac{1}{\delta}\left[G(V + a) - \dot{\delta}\right]\frac{\partial p}{\partial Y} + \frac{1}{r}\left(w + a \cos \beta_\varphi\right)\frac{\partial p}{\partial \Phi}\right\}$$

$$-\rho a\left\{\frac{1}{\lambda}\left(u + a \cos \beta_X\right)\frac{\partial V}{\partial X} + \frac{1}{\delta}\left[G(V + a) - \dot{\delta}\right]\frac{\partial V}{\partial Y} + \frac{1}{r}\left(w + a \cos \beta_\varphi\right)\frac{\partial V}{\partial \Phi}\right\}$$

$$-\rho a^2\left(\frac{1}{\lambda}\frac{\partial U_X}{\partial X} + \frac{1}{r}\frac{\partial U_\varphi}{\partial \Phi}\right) - \frac{\rho a}{\lambda}\left(av - u^2 \cos \beta_Y + uv \cos \beta_X\right)K$$

$$-\frac{\rho a}{r}\left[\left(av - w^2 \cos \beta_Y + vw \cos \beta_\varphi\right)\sin \theta + \left(au - w^2 \cos \beta_X + uw \cos \beta_\varphi\right)\cos \theta\right] \tag{33}$$

The quantities U_X and U_φ in equation (33) are the components of the shock tangential velocity component U in the x- and φ-directions, respectively. It can be determined from equation (29) and the vector relation

$$\vec{U} = \vec{e}_S \times \left(\vec{\frac{}{V}} \times \vec{e}_S\right)$$

that these quantities and the component U_Y satisfy the equations

$$\left.\begin{aligned} U_X &= u \sin^2 \beta_X - \cos \beta_X\left(v \cos \beta_Y + w \cos \beta_\varphi\right) \\ U_Y &= v \sin^2 \beta_Y - \cos \beta_Y\left(u \cos \beta_X + w \cos \beta_\varphi\right) \\ U_\varphi &= w \sin^2 \beta_\varphi - \cos \beta_\varphi\left(u \cos \beta_X + v \cos \beta_Y\right) \end{aligned}\right\} \tag{34}$$

It should be noted that the angles β_X, β_Y, and β_φ are evaluated at the shock point where the flow is being calculated and do not vary with X, Y, or Φ when the derivatives of V, U_X, and U_φ are being calculated. In other words, the only quantities in

equations (28) and (34) which are allowed to vary during the calculation of the derivatives are the velocity components u, v, and w. The form of equation (33) which is to be used at the axis (X = 0) for $\Phi = 0$ is

$$\frac{\partial p}{\partial \tau} + \rho a \frac{\partial V}{\partial \tau} = -\left\{\frac{1}{\lambda}\left(u + a \cos \beta_x\right)\frac{\partial p}{\partial X} + \frac{1}{\delta}\left[G(V + a) - \dot{\delta}\right]\frac{\partial p}{\partial Y}\right\}$$

$$- \rho a\left\{\frac{1}{\lambda}\left(u + a \cos \beta_x\right)\frac{\partial V}{\partial X} + \frac{1}{\delta}\left[G(V + a) - \dot{\delta}\right]\frac{\partial V}{\partial Y}\right\}$$

$$- \frac{\rho a^2}{\lambda}\frac{\partial}{\partial X}\left(U_x + u + \frac{\partial U_\varphi}{\partial \Phi}\right) - \frac{\rho a}{\lambda}\left(2av - u^2 \cos \beta_y + uv \cos \beta_x\right)K \qquad (35)$$

The solutions at the axis for other values of Φ are obtained from equations (16).

The present approach differs from the standard time-dependent method-of-characteristics approach at shock waves in that the characteristic compatibility relation given by equation (33) or (35) is integrated with finite-difference expressions. Central-difference formulas are used to evaluate the partial derivatives with respect to X and Φ, and backward-difference expressions are used to evaluate the derivatives with respect to Y. All these difference expressions are correct to second order. It should be noted that this modification of the method of characteristics is similar to that used by Masson, Taylor, and Foster (ref. 6) at the shock and body.

A two-step Brailovskaya scheme of the sort used in the shock layer and on the body surface is used to perform the integration. For the first step, the direction cosines of the normal to the bow shock wave and the free-stream direction and the shock angle σ are determined by using equations (24), (30), and (32). Then, the right side of equation (33) or (35) and the coefficient ρa on the left side are evaluated at time $\tau - \Delta\tau$. Let the right side of equation (33) or (35) be designated as R. The integrated compatibility equation for the first step is written as

$$p_I(\tau,X,1,\Phi) + \rho(\tau-\Delta\tau,X,1,\Phi)a(\tau-\Delta\tau,X,1,\Phi)V_I(\tau,X,1,\Phi)$$
$$= p(\tau-\Delta\tau,X,1,\Phi) + \rho(\tau-\Delta\tau,X,1,\Phi)a(\tau-\Delta\tau,X,1,\Phi)V(\tau-\Delta\tau,X,1,\Phi) + \Delta\tau R(\tau-\Delta\tau,X,1,\Phi) \qquad (36)$$

The subscript I used in equation (36) denotes the initial solution. This equation is solved simultaneously with the Rankine-Hugoniot relations (27) in order to determine an initial solution for the thermodynamic properties p, ρ, and $\tilde{\gamma}$, the velocity component V, and the shock velocity component $\dot{\delta}$ at time τ. If an equilibrium gas model is being treated, it is necessary to perform an iteration in order to obtain a converged

solution for the thermodynamic properties. The velocity components u, v, and w are determined with the equations

$$u = \overline{V}_\infty\left(\cos \alpha_x - \cos \sigma \cos \beta_x\right) + V \cos \beta_x$$

$$v = \overline{V}_\infty\left(\cos \alpha_y - \cos \sigma \cos \beta_y\right) + V \cos \beta_y$$

$$w = \overline{V}_\infty\left(\cos \alpha_\varphi - \cos \sigma \cos \beta_\varphi\right) + V \cos \beta_\varphi$$

For the second step, the right side of equation (33) or (35) and the quantity ρa are evaluated at time τ with the initial solution just obtained. The integrated compatibility relation is written as

$$p(\tau,X,1,\Phi) + \rho_I(\tau,X,1,\Phi)a_I(\tau,X,1,\Phi)V(\tau,X,1,\Phi)$$
$$= p(\tau-\Delta\tau,X,1,\Phi) + \rho_I(\tau,X,1,\Phi)a_I(\tau,X,1,\Phi)V(\tau-\Delta\tau,X,1,\Phi) + \Delta\tau R_I(\tau,X,1,\Phi)$$

This equation is then solved simultaneously with the Rankine-Hugoniot relations in the same manner as for the first step.

No damping terms are used at the shock wave since they proved to be unnecessary.

Starting Solution

It has been shown by a number of investigators that converged solutions for the steady supersonic blunt-body problem which have been calculated with time-dependent finite-difference methods are independent of the starting solution for all means and purposes. Thus, the starting solution can be quite approximate.

In this paper the starting solution is constructed from a specified axisymmetric shock wave with its axis in the free-stream direction and a specified surface pressure distribution and surface streamline pattern. It is assumed that the shock velocity for the initial solution is zero. Therefore, the complete solution at the shock can be determined with the Rankine-Hugoniot shock relations, the specified free-stream conditions, and the shock geometry.

The basic surface pressure distribution is the Newtonian one. At sharp corners for which the upstream value of the velocity component u is subsonic the pressure is adjusted so that u is equal to the local speed of sound. If the Newtonian pressure distribution does not indicate a stagnation point on the windward surface of the body (this happens, for example, for a flat-face cylinder at angle of attack), the stagnation pressure is imposed at the points with the largest Newtonian pressure, and the pressure at the other points is increased proportionally. In regions of wind shadow, the pressure is set equal to the pressure at the last point on the windward surface in the same φ-plane.

There is a provision for imposing a lower bound on the pressure at all points in the flow field.

The density at the surface is determined from the pressure distribution and the normal shock entropy. The use of normal shock entropy is considered reasonable since the results of Shifrin (ref. 16) suggest strongly that the maximum entropy streamline wets the surface when the flow field is not symmetric. The magnitude of the velocity $\overline{V}$ at the surface is determined from the pressure, density, and the total enthalpy. The surface components of velocity are obtained from the total velocity and the Newtonian surface streamlines which are used even in regions of wind shadow.

The flow properties at points between the shock and body are determined by linear interpolation. When an equilibrium gas model is to be used, the initial solution is calculated as a perfect gas. The value of $\tilde{\gamma}$ which is used is the normal shock value.

RESULTS AND DISCUSSION

In this section the results of the present method are compared with those of experiment and other methods for the flow of equilibrium air past the Apollo command module at the trim angle of attack and for perfect gas flow past a spherical cap and a spherically blunted cone at angle of attack. Both the cap and the cone are terminated with sharp shoulders. Results are presented also for perfect gas flow past a prolate spheroid with its major axis normal to the flow. In addition, several solutions for the flat-face cylinder at zero angle of attack which were obtained by using different finite-difference techniques are compared.

Smooth Bodies

Apollo command module.- The results of the present method for the bow-shock and sonic-line shapes and surface pressure distribution for the Apollo command module are compared with those of the inverse method of Webb, Dresser, Adler, and Waiter (ref. 17) in figure 7. The angle of attack is 22°, the flight velocity is 6935 m/s (22 754 ft/sec), and the altitude is 45.866 km (150 480 ft) in the atmosphere of the earth. For the present calculations, the free-stream properties at this altitude were obtained from reference 18 in terms of the geopotential altitude. It should be noted that since the Apollo command module is axisymmetric and has a generator composed of segments of constant curvature, it is well suited for treatment with the present method. The results of both methods are for air in thermodynamic equilibrium.

The shock- and sonic-line shapes presented in figure 7(a) are those in the plane of symmetry. The results of the present method and those of the inverse method (ref. 17) for the shock location and the sonic-line location in the windward semiplane ($\varphi = 180^{\circ}$)

coincide to within plotting accuracy. It is seen that the results of the two methods differ somewhat as to the location of the sonic line in the leeward semiplane ($\varphi = 0^{o}$).

The results for the pressure distribution for the plane of symmetry ($\varphi = 0^{o}$ and 180^{o}) and for the plane normal to the plane of symmetry ($\varphi = 90^{o}$) are compared in figure 7(b). It is seen that the difference in the sonic-line location in the leeward semiplane ($\varphi = 0^{o}$) is associated with only a small difference in the surface pressure distribution. This may be due to the fact that the value of the quantity $\tilde{\gamma} = h/e$ is close to 1. Since the gas is in thermodynamic equilibrium, the value of $\tilde{\gamma}$ varies somewhat over the flow field. However, in the subsonic region, the value of $\tilde{\gamma}$ is within 1 percent of the mean value of 1.145. It is seen in the figure that the inverse method predicts that the expansion at the corner in the plane $\varphi = 90^{o}$ starts closer to the axis than the present method does. It should be noted that difficulties are often experienced with the inverse method in the vicinity of shoulders.

The calculation presented in figure 7 for the Apollo command module was performed with a grid with seven semiplanes of constant φ so that $\Delta\Phi = 30^{o}$, three strips between the body and shock so that $\Delta Y = 1/3$, and nine mesh spacings ΔX along the generator of the reference surface. Five of these mesh spacings are on the arc subtending the face of the configuration, and the remaining four are on the arc subtending a portion of the shoulder. The time required to calculate the results of the present method shown in figure 7 on the CDC 6600 computer was 10 minutes. However, the results obtained after 5 minutes of calculation did not differ appreciably from the results presented in the figure. The inverse solution of reference 17 required many hours of computer time on the IBM 7094. A second calculation was made with the present method with a more refined grid. The results of this calculation did not differ appreciably from those presented in figure 7.

It was noted that the numerical solution is extremely sensitive to errors incurred by using too few φ-planes. An attempt was made to calculate the flow field about the Apollo command module by using the same grid as that just discussed except that five rather than seven planes of constant φ were used. This attempt was unsuccessful. The results obtained indicated that a pseudoseparation occurred on the shoulder on the leeward side of the body. First the cross-flow component of velocity w and then the u-component reversed directions near the shoulder. The total enthalpy increased in the region of reverse flow. Eventually, the calculation became unbounded.

Prolate spheroid.- In order to demonstrate the ability to compute flow about nonaxisymmetric bodies, two calculations with different mesh spacings were made for a prolate spheroid with its axis perpendicular to the flow. It should be noted that a prolate spheroid is a body of revolution with an ellipse for a generator and with the axis of revolution passing through the foci. For the first calculation, seven planes of constant φ

and three strips between the body and shock were used so that $\Delta\Phi = 30^{\circ}$ and $\Delta Y = 1/3$. Seven mesh spacings ΔX were used along the generator of the reference surface. For the second calculation, the mesh spacings $\Delta\Phi = 22.5^{\circ}$ and $\Delta Y = 1/5$ were used. Along the generator of the reference surface, 14 mesh spacings ΔX were employed. The bow-shock-wave and sonic-line shapes in the planes $\varphi = 0^{\circ}$ and $\varphi = 90^{\circ}$, which are normal to and contain the major axis, respectively, are shown in figure 8(a). The surface pressure distributions for these planes are shown in figure 8(b). Since the results of the two calculations are in good agreement, it can be concluded that convergence has been attained. Also shown in figure 8(b) is the Newtonian distribution. It is seen that the present results and the Newtonian results are in good agreement for the plane $\varphi = 0^{\circ}$ but differ somewhat for $\varphi = 90^{\circ}$.

Bodies With Sharp Shoulders

Flat-face cylinder.- In the Analysis section of this paper, it was indicated that a special procedure was needed in order to use finite-difference equations at sharp sonic shoulders. In order to demonstrate the need for the refinement, calculations were made for the flow past a flat-face cylinder at zero angle of attack with $M_{\infty} = 2.81$ and $\gamma = 1.4$ with both the modified and the unmodified procedures. The results for the surface pressure distribution and the pressure profile across the shock layer along a line normal to the face at the shoulder are presented in figure 9. The circles depict the results of the present method, which uses equations (23) at the shoulder when the upstream flow is subsonic, and the squares depict the results of a variation of the present method which uses equations (9) at the shoulder. The results depicted by the triangles were taken from reference 9 where the method of characteristics was used at the body surface. The experimental results of Kendall (ref. 19) are depicted by a solid line.

Since the present method employs equations (9) at all points except the shoulder, it might seem appropriate to use these equations at the shoulder also. However, it is seen from the figure that such a procedure does not predict the solution correctly at the shoulder. Both the present method and that of reference 9 are in fair agreement with experiment and each other, and the singular character of the flow at the shoulder is predicted correctly. It should be noted that the error in the results obtained with equations (9) at the shoulder is restricted to the neighborhood of the shoulder. In fact, it was found that the results of both the present method and its variation for the shock-wave and sonic-line locations agree with those of experiment and method of reference 9.

Spherical cap.- In figure 10, the results of the present method for a spherical cap with a sharp shoulder are compared with the experimental results of Stallings and Howell (ref. 20). The angle of attack is 15°, the free-stream Mach number is 2.49, and γ is 1.4. The radius of curvature of the cap is $\sqrt{2}r_b$. The shock-wave and sonic-line

locations in the plane of symmetry are shown in figure 10(a), the pressure distributions for the plane of symmetry ($\varphi = 0^o$ and $\varphi = 180^o$) and the plane normal to the plane of symmetry ($\varphi = 90^o$) are given in figure 10(b), and the distributions of the Mach number and the ratio u/a along the shoulder edge are given in figure 10(c). The mesh spacings $\Delta\Phi$ and ΔY have values of 22.5^o and 1/3, respectively. There were 15 mesh spacings ΔX along the generator of the reference surface.

The interest in calculating this particular case stems from the fact that experimental results show the flow at the shoulder to be sonic on the windward side of the body and supersonic on the leeward side. Therefore, this case provides a good test of the ability of the present method to calculate both sonic and supersonic shoulder flow. It is pointed out in the Analysis section that different computational procedures are used at sharp shoulders, depending upon whether the upstream flow is subsonic or supersonic. When the Mach number of the approaching flow is less than 1, equations (23) are used; when it is greater than 1, equations (9) are employed. It can be seen from the results presented in figure 10 that the present method predicts the character of the flow in the vicinity of the shoulder correctly.

Spherically blunted cone with sharp shoulder.- The results for the flow about a spherically blunted cone with a sharp shoulder are compared with the experimental results of Stallings and Tudor (ref. 21) in figure 11. The semiapex angle of the cone is 60^o, the ratio of nose radius to base radius is 0.25, the Mach number is 4.63, and the test gas is air. The values of angle of attack which are treated are 10^o and 20^o. The grid which is used for the $\alpha = 10^o$ calculations has 25 mesh spacings ΔX along the generator of the reference surface, four mesh spacings ΔY between the body and shock, and six mesh spacings $\Delta\Phi$ between $\varphi = 0^o$ and $\varphi = 180^o$. The grid used for $\alpha = 20^o$ has the same number of mesh spacings ΔX and ΔY and eight mesh spacings $\Delta\Phi$. Converged results were obtained for each of these cases in 300 time steps which corresponds to about 30 minutes of computer time.

The pressure distributions in the plane of symmetry are shown in figure 11(a). In addition to the results of the present method and experiment, the approximate solution obtained with a time-dependent, finite-difference method by Cohen, Foster, and Dowty (ref. 5) for a 10^o angle of attack is also presented. This method, which was discussed briefly in the Introduction, is basically the refined Godunov method of Masson, Taylor, and Foster (ref. 6). The flow is calculated in the plane of symmetry only, and the cross flow is assumed to vary as $\sin\varphi$. Two solutions for different values of the cross-flow weighting function are presented in reference 5. The solution presented in this paper is that designated as the ".433 crossflow approximation" in reference 5.

Several observations can be made concerning the results presented in figure 11(a). For the 10^o angle of attack, both the present method and the approximate method of

reference 5 show good agreement with experiment. Both methods indicate that the flow stagnates at a point on the spherical cap in agreement with experiment. It is seen that the present results indicate that the pressure on the cap is about 2 percent less than the exact stagnation value p_t. It should be noted that for the present method, four mesh spacings ΔX were used between the geometrical stagnation point and the edge of the spherical cap. It is believed that better agreement with experiment would have been achieved had more mesh spacings been used on the cap. Six mesh spacings were used on the cap for the calculation of reference 5, and excellent agreement with experiment was achieved. It is seen that a discontinuity in the pressure gradient at the junction of the cap and cone in the plane of symmetry is predicted by both methods for both the windward and leeward sides.

The results of the present method for the 20^o angle of attack are in good agreement with experiment except near the shoulder on the leeward side where an irregularity in the present results for the pressure distribution occurs. This irregularity occurs concurrently with a nonphysical variation of the surface entropy of 4 percent near the corner. The irregularity does not affect the Mach number distribution adversely as it does the pressure distribution. The computed Mach number at the leeward corner is 0.969, which is reasonably close to 1, and the Mach number computed at grid points in the leeward plane upstream of the shoulder decreases monotonically as it should but remains close to 1 for some distance. The present results show that the stagnation point is located on the conical surface in the windward plane in agreement with experiment.

It was stated in reference 5 that a calculation was made for a 20^o angle of attack but that the results did not agree with experiment. It was reported that the stagnation point was located on the spherical cap in the windward plane rather than on the cone. The results of the present method give an indication as to why the approximate method of reference 5 was successful for a 10^o angle of attack and unsuccessful for 20^o. The peripheral distribution of the cross flow along the edge and along the junction of the cap and cone are shown for 10^o and 20^o angles of attack in figures 11(b) and 11(c), respectively. Also shown in these figures are the distributions of the form

$$w = w_{90^o} \sin \varphi$$

which is the form assumed in reference 5. It is seen that for a 10^o angle of attack, the computed cross flow varies as $\sin \varphi$ both at the edge and at the junction. For a 20^o angle of attack, the cross flow at the edge varies as $\sin \varphi$, but at the junction in the nose region the computed cross-flow solution and the trigonometric function differ slightly. Apparently the solutions for the various flow properties in the stagnation region are strongly coupled so that even a small deviation in the cross-flow velocity distribution has a marked effect on the other properties.

The peripheral pressure distributions for three values of s/r_b are shown for 10^o and 20^o angles of attack in figures 11(d) and 11(e), respectively. The values of s/r_b are 0.10, 0.45, and 0.90 and were chosen because there are both computational points and experimental orifices very close to these locations. The first ring $(s/r_b = 0.10)$ is located on the spherical cap near the junction with the cone, the second ring $(s/r_b = 0.45)$ is located on the cone and is closer to the junction than the edge, and the third ring $(s/r_b = 0.90)$ is located on the cone near the edge. It is seen in figures 11(d) and 11(e) that the results for both angles of attack are in fair agreement with experiment but that the present and experimental results for the 10^o angle of attack are in closer agreement than those for 20^o. It should be pointed out that at the location $s/r_b = 0.10$ where the comparison is made on the cap, there is more difference between theory and experiment than at the other computational points on the cap, as can be seen in figure 11(a).

In figure 11(d), results are presented for two calculations for the 10^o angle of attack. For one calculation the mesh spacing $\Delta\Phi$ has a value of 30^o, whereas for the other calculation the value of $\Delta\Phi$ is 45^o. The number and size of the mesh spacings ΔX and ΔY are the same for both calculations. The results of the calculation with $\Delta\Phi = 30^o$ are the ones presented in the rest of figure 11. A comparison of the results of the two calculations presented in figure 11(d) shows that the solution is converged near the edge $(s/r_b = 0.90)$ for all values of φ. It is also converged on the leeward side for all values of s. However, it is seen that a refining of the grid does improve the results at other points on the surface.

It was shown in the Analysis section that the cross flow should not exhibit singular behavior at sonic shoulders although the other flow properties do show singular behavior at these shoulders. In order to show that the numerical solution does, in fact, behave in this manner, the results at 10^o and 20^o angles of attack for the pressure, velocity component u, and cross-flow component w in the plane $\varphi = 90^o$ are shown in figures 11(f), 11(g), and 11(h), respectively. It is seen that both the pressure and the velocity component u have steep gradients at the shoulder whereas the cross flow does not.

CONCLUDING REMARKS

A two-step, time-dependent method of second-order accuracy for calculating supersonic flow about nonaxisymmetric blunt bodies and axisymmetric blunt bodies with sharp shoulders is presented. The bow shock wave is treated as a discontinuity, and a modification to the time-dependent method of characteristics is used to determine the solution at the shock. Finite-difference techniques are used to calculate the solution at the body surface and in the shock layer between the shock and surface. An approximate finite-difference method for use at sharp sonic shoulders is presented. A stability analysis of the finite-difference method is given.

Comparisons of the results of the present method with experiment and the results of other methods are made for the flow of equilibrium air past the Apollo command module at the trim angle of attack and for perfect gas flow past a spherical cap and a spherically blunted cone at angle of attack. Both the cap and the blunted cone are terminated with sharp shoulders. In general, the agreement with other results is good. Results are presented also for perfect gas flow past a prolate spheroid with its major axis normal to the flow.

It is found that time-dependent methods which employ only finite-difference integration techniques can be used to calculate numerical solutions at sharp shoulders where the flow is singular. In particular, finite-difference techniques can be used to integrate the compatibility relation which is employed in conjunction with the Rankine-Hugoniot relations in the time-dependent method-of-characteristics solution at the bow shock wave. Thus, it is not necessary to construct the characteristics network that would otherwise be required.

The present solutions account for the cross flow at the shoulder. It is shown that when there is cross flow at the shoulder, the sonic or supersonic nature of the solution depends upon whether the component of velocity tangent to the surface and normal to the shoulder edge is subsonic or supersonic upstream of the shoulder. The properties which are singular at a sonic shoulder are the component of velocity just discussed and the thermodynamic properties; the cross flow is not singular.

It is demonstrated that numerical solutions for supersonic flow about blunt bodies at angle of attack can be obtained in a reasonable amount of computer time. For example, the flow field with real-gas effects about the Apollo command module at the trim angle of attack was calculated in 10 minutes on the CDC 6600 computer.

Langley Research Center,
National Aeronautics and Space Administration,
Hampton, Va., May 25, 1971.

APPENDIX A

CURVE FIT FOR THE THERMODYNAMIC FUNCTION $\tilde{\gamma}(\rho,e)$ FOR EQUILIBRIUM AIR

The data of Allison (ref. 22) and Browne (ref. 23) have been used to construct this curve fit for the function $\tilde{\gamma} = h/e$ for equilibrium air. The independent variables are the density ρ and the internal energy e. The ranges of these variables for which the curve fit applies are

$$10^{-4} \leqq \frac{\rho}{\rho_o} \leqq 10 \qquad\qquad \frac{e}{RT_o} \leqq 1500$$

The heat of formation of the gas must be adjusted so that $h = e = 0$ at a temperature of absolute zero.

The curve fit is given by the following equations:

$$\tilde{\gamma} = 1.405 \qquad \left(\log_{10}\frac{e}{RT_o} \leqq 0.801\right)$$

$$\tilde{\gamma} = 1.5055 - 0.1255 \log_{10}\frac{e}{RT_o} \qquad \left(0.801 < \log_{10}\frac{e}{RT_o} \leqq 2.300;\ \log_{10}\frac{\rho}{\rho_o} \geqq \frac{3.255 - 2.278\log_{10}\frac{e}{RT_o}}{1 - 0.822\log_{10}\frac{e}{RT_o}}\right)$$

$$\tilde{\gamma} = \left(1.6370 - 0.0404\log_{10}\frac{\rho}{\rho_o}\right) - \left(0.2175 - 0.0332\log_{10}\frac{\rho}{\rho_o}\right)\log_{10}\frac{e}{RT_o} - \frac{\left(0.1366 - 0.0366\log_{10}\frac{\rho}{\rho_o}\right) - \left(0.0833 - 0.0248\log_{10}\frac{\rho}{\rho_o}\right)\log_{10}\frac{e}{RT_o}}{1 + \exp\left[-18.30\left(\log_{10}\frac{e}{RT_o} - 0.0320\log_{10}\frac{\rho}{\rho_o} - 1.943\right)\right]}$$

$$\left(0.801 < \log_{10}\frac{e}{RT_o} \leqq 2.300;\ \log_{10}\frac{\rho}{\rho_o} < \frac{3.255 - 2.278\log_{10}\frac{e}{RT_o}}{1 - 0.822\log_{10}\frac{e}{RT_o}}\right)$$

$$\tilde{\gamma} = \left(1.5004 - 0.0038\log_{10}\frac{\rho}{\rho_o}\right) - \left(0.1342 - 0.0084\log_{10}\frac{\rho}{\rho_o}\right)\log_{10}\frac{e}{RT_o} - \frac{\left(0.3274 + 0.0091\log_{10}\frac{\rho}{\rho_o}\right) - \left(0.1342 + 0.0016\log_{10}\frac{\rho}{\rho_o}\right)\log_{10}\frac{e}{RT_o}}{1 + \exp\left[-15.85\left(\log_{10}\frac{e}{RT_o} - 0.0320\log_{10}\frac{\rho}{\rho_o} - 2.708\right)\right]}$$

$$\left(2.300 < \log_{10}\frac{e}{RT_o} \leqq 3.176\right)$$

The quantity ρ_o is the reference density and has a value of 1.292 kg/m^3 (2.507×10^{-3} slug/ft^3). The quantities R and T_o are the gas constant for air and the freezing temperature at 1 atmosphere of pressure; the product RT_o has a value of 78.40 kJ/kg (8.439×10^5 ft^2/sec^2).

APPENDIX B

STABILITY ANALYSIS FOR FINITE-DIFFERENCE EQUATIONS

In this appendix the Von Neumann condition for the linearized form of the present finite-difference equations is determined. This condition specifies the upper bound for the mesh spacing $\Delta\tau$ above which it may be expected that the magnitude of a given infinitesimal error will increase at successive time steps. In general, difference schemes which amplify small errors produce solutions which either diverge or contain large errors.

The basic procedure which is used here is similar to that of reference 9 and is based on the earlier work of Richtmyer (ref. 24). A technique employed by Van Leer (ref. 25) is used to account for the difference in the mesh spacing sizes for the X-, Y-, and Φ-coordinates. This treatment accounts for the nonorthogonal nature of the X,Y,Φ coordinate system. A nonphysical dissipation function of fourth order similar to that used by Richtmyer and Morton (ref. 12) is employed to avoid neutral stability.

The partial differential equations (2) and (4b) can be written in matrix form in terms of the coordinates τ, X, Y, and Φ as

$$\frac{\partial W}{\partial \tau} + \frac{\tilde{A}}{\lambda}\frac{\partial W}{\partial X} + \frac{\tilde{B}}{\delta}\frac{\partial W}{\partial Y} + \frac{\tilde{C}}{r}\frac{\partial W}{\partial \Phi} + \tilde{D} = 0 \tag{B1}$$

where the vectors W and $\tilde{D}$ and the matrices $\tilde{A}$, $\tilde{B}$, and $\tilde{C}$ are as follows:

$$W = \begin{Bmatrix} \rho \\ u \\ v \\ w \\ p \end{Bmatrix} \qquad \tilde{D} = \left\{ \begin{Bmatrix} \rho u \dfrac{\cos\theta}{r} + \rho v\left(\dfrac{K}{\lambda} + \dfrac{\sin\theta}{r}\right) \\ uv\dfrac{K}{\lambda} - w^2\dfrac{\cos\theta}{r} \\ -u^2\dfrac{K}{\lambda} - w^2\dfrac{\sin\theta}{r} \\ uw\dfrac{\cos\theta}{r} + vw\dfrac{\sin\theta}{r} \\ \rho u a^2\dfrac{\cos\theta}{r} + \rho v a^2\left(\dfrac{K}{\lambda} + \dfrac{\sin\theta}{r}\right) \end{Bmatrix} \right\} \tag{B2}$$

(Equations continued on next page)

APPENDIX B

$$
\left.
\begin{aligned}
\tilde{A} &= \begin{bmatrix} u & \rho & 0 & 0 & 0 \\ 0 & u & 0 & 0 & \frac{1}{\rho} \\ 0 & 0 & u & 0 & 0 \\ 0 & 0 & 0 & u & 0 \\ 0 & \rho a^2 & 0 & 0 & u \end{bmatrix} \\
\tilde{B} &= \begin{bmatrix} \tilde{v} & -\frac{\left(Y\delta' + y_b'\right)\rho}{\lambda} & \rho & -\frac{\left(Y\hat{\delta} + \hat{y}_b\right)\rho}{r} & 0 \\ 0 & \tilde{v} & 0 & 0 & -\frac{\left(Y\delta' + y_b'\right)}{\rho\lambda} \\ 0 & 0 & \tilde{v} & 0 & \frac{1}{\rho} \\ 0 & 0 & 0 & \tilde{v} & -\frac{\left(Y\hat{\delta} + \hat{y}_b\right)}{\rho r} \\ 0 & -\frac{\left(Y\delta' + y_b'\right)\rho a^2}{\lambda} & \rho a^2 & -\frac{\left(Y\hat{\delta} + \hat{y}_b\right)\rho a^2}{r} & \tilde{v} \end{bmatrix} \\
\tilde{C} &= \begin{bmatrix} w & 0 & 0 & \rho & 0 \\ 0 & w & 0 & 0 & 0 \\ 0 & 0 & w & 0 & 0 \\ 0 & 0 & 0 & w & \frac{1}{\rho} \\ 0 & 0 & 0 & \rho a^2 & w \end{bmatrix}
\end{aligned}
\right\} \qquad \text{(B2)}
$$

where

$$
\tilde{v} = v - \left[Y\dot{\delta} + \frac{\left(Y\delta' + y_b'\right)u}{\lambda} + \frac{\left(Y\hat{\delta} + \hat{y}_b\right)w}{r} \right] \qquad \text{(B3)}
$$

The finite-difference representations of equations (B1) for the initial and final steps of the Brailovskaya scheme are written as

APPENDIX B

$$W_I(\tau,X,Y,\Phi) = W(\tau-\Delta\tau,X,Y,\Phi) - \left\{ \frac{\tilde{A}}{\lambda}\left[\frac{W(\tau-\Delta\tau,X+\Delta X,Y,\Phi) - W(\tau-\Delta\tau,X-\Delta X,Y,\Phi)}{2\,\Delta X}\right] + \frac{\tilde{B}}{\delta}\left[\frac{W(\tau-\Delta\tau,X,Y+\Delta Y,\Phi) - W(\tau-\Delta\tau,X,Y-\Delta Y,\Phi)}{2\,\Delta Y}\right] + \frac{\tilde{C}}{r}\left[\frac{W(\tau-\Delta\tau,X,Y,\Phi+\Delta\Phi) - W(\tau-\Delta\tau,X,Y,\Phi-\Delta\Phi)}{2\,\Delta\Phi}\right] + \tilde{D}\right\}\Delta\tau \tag{B4}$$

and

$$\begin{aligned} W(\tau,X,Y,\Phi) = W(\tau-\Delta\tau,X,Y,\Phi) &- \left\{ \frac{\tilde{A}}{\lambda}\left[\frac{W_I(\tau,X+\Delta X,Y,\Phi) - W_I(\tau,X-\Delta X,Y,\Phi)}{2\,\Delta X}\right] \right. \\ &+ \frac{\tilde{B}}{\delta}\left[\frac{W_I(\tau,X,Y+\Delta Y,\Phi) - W_I(\tau,X,Y-\Delta Y,\Phi)}{2\,\Delta Y}\right] \\ &\left. + \frac{\tilde{C}}{r}\left[\frac{W_I(\tau,X,Y,\Phi+\Delta\Phi) - W_I(\tau,X,Y,\Phi-\Delta\Phi)}{2\,\Delta\Phi}\right] + \tilde{D}\right\}\Delta\tau \\ &- \epsilon\left[W(\tau-\Delta\tau,X+2\Delta X,Y,\Phi) - 4W(\tau-\Delta\tau,X+\Delta X,Y,\Phi) + 6W(\tau-\Delta\tau,X,Y,\Phi)\right. \\ &- 4W(\tau-\Delta\tau,X-\Delta X,Y,\Phi) + W(\tau-\Delta\tau,X-2\Delta X,Y,\Phi) \\ &+ W(\tau-\Delta\tau,X,Y+2\Delta Y,\Phi) - 4W(\tau-\Delta\tau,X,Y+\Delta Y,\Phi) + 6W(\tau-\Delta\tau,X,Y,\Phi) \\ &- 4W(\tau-\Delta\tau,X,Y-\Delta Y,\Phi) + W(\tau-\Delta\tau,X,Y-2\Delta Y,\Phi) \\ &+ W(\tau-\Delta\tau,X,Y,\Phi+2\Delta\Phi) - 4W(\tau-\Delta\tau,X,Y,\Phi+\Delta\Phi) + 6W(\tau-\Delta\tau,X,Y,\Phi) \\ &\left. - 4W(\tau-\Delta\tau,X,Y,\Phi-\Delta\Phi) + W(\tau-\Delta\tau,X,Y,\Phi-2\Delta\Phi)\right] \end{aligned} \tag{B5}$$

The subscript I in equations (B4) and (B5) indicates the initial solution. The matrices $\tilde{A}$, $\tilde{B}$, and $\tilde{C}$ and the vector $\tilde{D}$ are evaluated at the point $(\tau - \Delta\tau,X,Y,\Phi)$.

It is assumed that the solution is of the form

$$W(\tau+\Delta\tau,X\pm\Delta X,Y\pm\Delta Y,\Phi\pm\Delta\Phi) = W(\tau,X,Y,\Phi)\exp\left[\tilde{\alpha}\,\Delta\tau \pm i(\eta + \xi + \psi)\right] \tag{B6}$$

where

$$\eta = \frac{2\pi}{L_x}\Delta X \qquad \xi = \frac{2\pi}{L_y}\Delta Y \qquad \psi = \frac{2\pi}{L_\varphi}\Delta\Phi \tag{B7}$$

and i is $\sqrt{-1}$. The quantities L_x, L_y, and L_φ are the wavelengths of the error solutions in the X-, Y-, and Φ-directions, respectively. Define the quantities r_1, r_2, and r_3 as

$$r_1 = \frac{\Delta\tau}{\lambda\,\Delta X} \qquad r_2 = \frac{\Delta\tau}{\delta\,\Delta Y} \qquad r_3 = \frac{\Delta\tau}{r\,\Delta\Phi} \tag{B8}$$

and assume that $\Delta\tau$ is small so that the term $\tilde{D}\,\Delta\tau$ can be neglected. By using equations (B6) to (B8), equations (B4) and (B5) can be written as

$$W_I(\tau,X,Y,\Phi) = \tilde{e}W(\tau-\Delta\tau,X,Y,\Phi) = \tilde{E}W(\tau-\Delta\tau,X,Y,\Phi) \tag{B9}$$

and

$$W(\tau,X,Y,\Phi) = \tilde{g}W(\tau-\Delta\tau,X,Y,\Phi) = \tilde{G}W(\tau-\Delta\tau,X,Y,\Phi) \tag{B10}$$

respectively, where the matrices $\tilde{E}$ and $\tilde{G}$ are given by the respective equations

$$\tilde{E} = r_1\tilde{A}\sin\eta + r_2\tilde{B}\sin\xi + r_3\tilde{C}\sin\psi \tag{B11}$$

and

$$\tilde{G} = (1 - \epsilon f)I - \tilde{E}^2 - i\tilde{E} \tag{B12}$$

where

$$f = 4\left[(1-\cos\eta)^2 + (1-\cos\xi)^2 + (1-\cos\psi)^2\right] \tag{B13}$$

The quantity I is the identity matrix. The numbers $\tilde{e}$ and $\tilde{g}$ are both defined as $\exp(\tilde{\alpha}\,\Delta\tau)$ although they are not equal since the quantity $\tilde{\alpha}$ is not the same for the first- and the second-step solutions. The equations (B9) and (B10) can be written in the forms

$$(\tilde{E} - I\tilde{e})W = 0 \qquad (\tilde{G} - I\tilde{g})W = 0$$

APPENDIX B

For nontrivial solutions of W, the determinant of the coefficients of the components of W in these equations must vanish; that is

$$\left|\tilde{E} - I\tilde{e}\right| = 0 \qquad \left|\tilde{G} - I\tilde{g}\right| = 0 \tag{B14}$$

Equations (B14) can be used to determine the eigenvalues $\tilde{e}$ and $\tilde{g}$ of the matrices $\tilde{E}$ and $\tilde{G}$, respectively.

First consider the matrix $\tilde{E}$. Let the quantities m, $\cos \mu_1$, $\cos \mu_2$, $\cos \mu_3$, and $\tilde{U}$ be defined as

$$\left.\begin{aligned}
m &= \sqrt{\left[r_1 \sin \eta - \frac{r_2\left(Y\delta' + y_b'\right)\sin \xi}{\lambda}\right]^2 + r_2^2 \sin^2 \xi + \left[r_3 \sin \psi - \frac{r_2\left(Y\hat{\delta} + \hat{y}_b\right)\sin \xi}{r}\right]^2} \\
\cos \mu_1 &= \frac{r_1 \sin \eta - \dfrac{r_2\left(Y\delta' + y_b'\right)\sin \xi}{\lambda}}{m} \\
\cos \mu_2 &= \frac{r_2 \sin \xi}{m} \\
\cos \mu_3 &= \frac{r_3 \sin \psi - \dfrac{r_2\left(Y\hat{\delta} + \hat{y}_b\right)\sin \xi}{r}}{m} \\
\tilde{U} &= u \cos \mu_1 + \left(v - Y\dot{\delta}\right)\cos \mu_2 + w \cos \mu_3
\end{aligned}\right\} \tag{B15}$$

The matrix $\tilde{E}$ can be written in terms of these quantities as

$$\tilde{E} = \begin{bmatrix}
\tilde{U} & \rho \cos \mu_1 & \rho \cos \mu_2 & \rho \cos \mu_3 & 0 \\
0 & \tilde{U} & 0 & 0 & \dfrac{\cos \mu_1}{\rho} \\
0 & 0 & \tilde{U} & 0 & \dfrac{\cos \mu_2}{\rho} \\
0 & 0 & 0 & \tilde{U} & \dfrac{\cos \mu_3}{\rho} \\
0 & \rho a^2 \cos \mu_1 & \rho a^2 \cos \mu_2 & \rho a^2 \cos \mu_3 & \tilde{U}
\end{bmatrix} \tag{B16}$$

APPENDIX B

By using the first of equations (B14) and equation (B16), the eigenvalues of the matrix $\tilde{E}$ are

$$\tilde{e} = m\bar{e} = m\tilde{U},m\tilde{U},m\tilde{U},m(\tilde{U} + a),m(\tilde{U} - a) \tag{B17}$$

It should be noted that

$$\bar{e} \leqq \bar{e}_{max} = \left|\tilde{U}\right| + a$$

It can be shown from equations (B12) and (B14) that the eigenvalue of the matrix $\tilde{G}$ can be expressed as

$$\tilde{g} = 1 - \epsilon f - \tilde{e}^2 - i\tilde{e}$$

The stability condition which is used in this paper is that the magnitude of $\tilde{g}$ should not exceed 1. This condition is expressed as

$$\left|\tilde{g}\right|^2 = \left(1 - \tilde{e}^2 - \epsilon f\right)^2 + \tilde{e}^2 \leqq 1 \tag{B18}$$

Consider what happens if $\tilde{e} = 0$, and note from equation (B13) that $0 \leqq f \leqq 48$. It is seen from these conditions and the inequality (B18) that ϵ must satisfy the inequalities

$$0 \leqq \epsilon \leqq \epsilon_{max} = \frac{1}{24} \tag{B19}$$

The inequality (B18) can be rewritten as

$$F_l = \left(\frac{1}{2} - \epsilon f\right) - \sqrt{\frac{1}{4} + \epsilon f} \leqq \tilde{e}^2 \leqq \left(\frac{1}{2} - \epsilon f\right) + \sqrt{\frac{1}{4} + \epsilon f} = F_u \tag{B20}$$

where F_l and F_u are the lower and upper bounds of $\tilde{e}^2$. It can be shown that for the values of ϵ in inequality (B19) the lower bound has a maximum value of zero. Thus the inequality can be rewritten as

$$0 \leqq m^2\bar{e}^2 \leqq F_u \tag{B21}$$

APPENDIX B

From the first of equations (B15) it is seen that m must satisfy the inequality

$$m^2 \leq \left(r_1 \left| \sin \eta \right| + \frac{r_2 \left| \sin \xi \right| \left| Y\delta' + y_b' \right|}{\lambda} \right)^2 + r_2^2 \sin^2 \xi + \left(r_3 \left| \sin \psi \right| + \frac{r_2 \left| \sin \xi \right| \left| Y\hat{\delta} + \hat{y}_b \right|}{r} \right)^2$$

$$\leq \tilde{m}^2 r_{max}^2 \left[\sin^2 \eta + \sin^2 \xi + \sin^2 \psi \right]$$

where

$$\left.
\begin{aligned}
\tilde{m}^2 &= \left(\cos \nu_1 + P_1 \cos \nu_2 \right)^2 + \cos \nu_2^2 + \left(\cos \nu_3 + P_3 \cos \nu_2 \right)^2 \\
\cos \nu_1 &= \frac{r_1 \left| \sin \eta \right|}{\sqrt{r_1^2 \sin^2 \eta + r_2^2 \sin^2 \xi + r_3^2 \sin^2 \psi}} \\
\cos \nu_2 &= \frac{r_2 \left| \sin \xi \right|}{\sqrt{r_1^2 \sin^2 \eta + r_2^2 \sin^2 \xi + r_3^2 \sin^2 \psi}} \\
\cos \nu_3 &= \frac{r_3 \left| \sin \psi \right|}{\sqrt{r_1^2 \sin^2 \eta + r_2^2 \sin^2 \xi + r_3^2 \sin^2 \psi}} \\
P_1 &= \frac{\left| Y\delta' + y_b' \right|}{\lambda} \\
P_3 &= \frac{\left| Y\hat{\delta} + \hat{y}_b \right|}{r}
\end{aligned}
\right\} \qquad \text{(B22)}$$

The quantity r_{max} is simply the largest of r_1, r_2, and r_3. It can be shown that the quantity $\tilde{m}$ satisfies the inequality

APPENDIX B

$$\tilde{m}^2 = 1 + \frac{1}{2}\left(P_1^2 + P_3^2\right)\left(1 + \cos 2\nu_2\right) + 2\left(P_1 \cos \nu_1 + P_3 \cos \nu_3\right)\cos \nu_2$$

$$\leq \frac{1}{2}\left(2 + P_1^2 + P_3^2\right) + \frac{1}{2}\left(P_1^2 + P_3^2\right)\cos 2\nu_2 + \sqrt{P_1^2 + P_3^2}\,\sin 2\nu_2$$

$$\leq \frac{1}{2}\left(2 + P_1^2 + P_3^2\right) + \frac{1}{2}\sqrt{P_1^2 + P_3^2}\sqrt{4 + P_1^2 + P_3^2}$$

$$= \left(1 + \frac{1}{2}Q^2\right) + \frac{1}{2}Q\sqrt{4 + Q^2}$$

where the quantity Q is defined by the equation

$$Q = \sqrt{P_1^2 + P_3^2} = \sqrt{\frac{1}{\lambda^2}\left(Y\delta' + y_b'\right)^2 + \frac{1}{r^2}\left(Y\hat{\delta} + \hat{y}_b\right)^2} \tag{B23}$$

It can be seen from equation (B13) that the quantity f can be written as

$$f = 16\left(\sin^4 \frac{\eta}{2} + \sin^4 \frac{\xi}{2} + \sin^4 \frac{\psi}{2}\right) = 48\chi^2$$

where $0 \leq \chi \leq 1$. Let $\bar{\epsilon}$ be defined as

$$\bar{\epsilon} = \epsilon / \epsilon_{max} = 24\epsilon$$

The upper bound F_u of $\tilde{e}^2$ can be written as

$$F_u\left(\chi, \bar{\epsilon}\right) = \left(\frac{1}{2} - 2\bar{\epsilon}\chi^2\right) + \sqrt{\frac{1}{4} + 2\bar{\epsilon}\chi^2}$$

At this point, it should be noted that

$$\left(\sin^2 \frac{\eta}{2} + \sin^2 \frac{\xi}{2} + \sin^2 \frac{\psi}{2}\right)^2 = \sin^4 \frac{\eta}{2} + \sin^4 \frac{\xi}{2} + \sin^4 \frac{\psi}{2}$$

$$+ 2\left(\sin^2 \frac{\eta}{2}\sin^2 \frac{\xi}{2} + \sin^2 \frac{\eta}{2}\sin^2 \frac{\psi}{2} + \sin^2 \frac{\xi}{2}\sin^2 \frac{\psi}{2}\right)$$

$$\leq 3\left(\sin^4 \frac{\eta}{2} + \sin^4 \frac{\xi}{2} + \sin^4 \frac{\psi}{2}\right)$$

$$= 9\chi^2$$

It follows that

$$\sin^2\eta + \sin^2\xi + \sin^2\psi = 4\left[\left(\sin^2\frac{\eta}{2} + \sin^2\frac{\xi}{2} + \sin^2\frac{\psi}{2}\right) - \left(\sin^4\frac{\eta}{2} + \sin^4\frac{\xi}{2} + \sin^4\frac{\psi}{2}\right)\right] \leqq 12(\chi - \chi^2)$$

Therefore, the inequality (B21) can be rewritten as

$$r_{max}^2 \leqq \frac{F_u}{\bar{e}_{max}^2 \tilde{m}^2\left(\sin^2\eta + \sin^2\xi + \sin^2\psi\right)} = \frac{\overline{F}_u^2(\chi,\bar{\epsilon})}{3\bar{e}_{max}^2\left[1 + \frac{1}{2}Q\left(Q + \sqrt{4 + Q^2}\right)\right]}$$

where

$$\overline{F}_u(\chi,\bar{\epsilon}) = \frac{1}{2}\sqrt{\frac{\left(\frac{1}{2} - 2\bar{\epsilon}\chi^2\right) + \sqrt{\frac{1}{4} + 2\bar{\epsilon}\chi^2}}{\chi - \chi^2}} \tag{B24}$$

For each value of $\bar{\epsilon}$ between 0 and 1, the function $\overline{F}_u(\chi,\bar{\epsilon})$ reaches a minimum value for some particular value of χ between 1/2 and 1. The minimizing values of $\bar{\epsilon}$ and χ are related by the equation

$$\bar{\epsilon} = \frac{4\chi^2 + 8\chi - 5 + \sqrt{16\chi^4 + 64\chi^3 + 24\chi^2 - 16\chi - 7}}{16\chi^2}$$

The least upper bound of $\overline{F}_u(\chi,\bar{\epsilon})$ for each value of $\bar{\epsilon}$ is designated as $\bar{f}_u(\bar{\epsilon})$. This function, which varies monotonically from a value of 1 at $\bar{\epsilon} = 0$ to a value of $\sqrt{2/3}$ at $\bar{\epsilon} = 1$, is plotted in figure 12.

In the situation encountered in this paper, the shock velocities are relatively small. Thus, the effective upper bound of $\tilde{U}$ is the magnitude of the total velocity $\overline{V}$; that is

$$\tilde{U} \approx u\cos\mu_1 + v\cos\mu_2 + w\cos\mu_3 \leqq \overline{V} = \sqrt{u^2 + v^2 + w^2}$$

and the quantity $\overline{V} + a$ is the effective upper bound of $\bar{e}_{max} = \left|\tilde{U}\right| + a$.

It follows from the analysis presented in this appendix that the Von Neumann condition for stability for the present finite-difference scheme is expressed by the inequality

$$\Delta\tau \leqq \frac{\bar{f}_u(\epsilon)\min(\lambda\,\Delta X, \delta\,\Delta Y, r\,\Delta\Phi)}{\sqrt{3}(\overline{V} + a)\sqrt{1 + \frac{1}{2}Q\left(Q + \sqrt{4 + Q^2}\right)}}$$

APPENDIX C

THE CHARACTERISTIC COMPATIBILITY RELATION

There are a number of treatments of the multidimensional method of characteristics. The analysis presented here follows the treatment of Von Mises (ref. 26).

Consider a multidimensional space. Compatibility relations for this space are linear combinations of the equations of motion which can be expressed in terms of total derivatives along given lines called a bicharacteristics and partial derivatives in terms of some of the independent variables. It should be noted that compatibility relations do not exist for all flow fields. However, if one of the independent variables is time and the flow field is inviscid, compatibility relations always exist. The total derivatives in these relations are with respect to time, and there are no partial derivatives with respect to time.

The space which is used in this paper is four dimensional, and the independent variables are time t and the coordinates x, y, and φ. The equations of motion which are combined linearly to form compatibility relations along the acoustic bicharacteristics are equations (2b), (2c), (2d), and (4b).

Let the direction cosines of the bicharacteristic in t,x,y,φ space along which a compatibility relation applies be h_t, h_x, h_y, and h_φ. By using the techniques discussed in reference 26, it can be shown that there is a family of bicharacteristics through each point in t,x,y,φ space, the members of which have direction cosines which satisfy the equation

$$h_t + uh_x + vh_y + wh_\varphi = \pm a\sqrt{h_x^2 + h_y^2 + h_\varphi^2} \tag{C1}$$

Let the constants of proportionality for equations (2b), (2c), (2d), and (4b) in the compatibility relations be a_1, a_2, a_3, and a_4, respectively. It can be shown that a_1, a_2, and a_3 are related to a_4 by the equations

$$\left.\begin{aligned} a_1 &= -\frac{\rho a^2 h_x}{h_t + uh_x + vh_y + wh_\varphi}\, a_4 \\ a_2 &= -\frac{\rho a^2 h_y}{h_t + uh_x + vh_y + wh_\varphi}\, a_4 \\ a_3 &= -\frac{\rho a^2 h_\varphi}{h_t + uh_x + vh_y + wh_\varphi}\, a_4 \end{aligned}\right\} \tag{C2}$$

APPENDIX C

By using equations (C1) and (C2), the compatibility relations can be written as

$$\mp\rho a \frac{h_x}{\sqrt{h_x^2 + h_y^2 + h_\varphi^2}}\left(\frac{\partial u}{\partial t} + \frac{u}{\lambda}\frac{\partial u}{\partial x} + v\frac{\partial u}{\partial y} + \frac{w}{r}\frac{\partial u}{\partial \varphi} + \frac{1}{\rho\lambda}\frac{\partial p}{\partial x} + \frac{K}{\lambda}uv - \frac{\cos\theta}{r}w^2\right)$$

$$\mp \rho a \frac{h_y}{\sqrt{h_x^2 + h_y^2 + h_\varphi^2}}\left(\frac{\partial v}{\partial t} + \frac{u}{\lambda}\frac{\partial v}{\partial x} + v\frac{\partial v}{\partial y} + \frac{w}{r}\frac{\partial v}{\partial \varphi} + \frac{1}{\rho}\frac{\partial p}{\partial y} - \frac{K}{\lambda}u^2 - \frac{\sin\theta}{r}w^2\right)$$

$$\mp \rho a \frac{h_\varphi}{\sqrt{h_x^2 + h_y^2 + h_\varphi^2}}\left(\frac{\partial w}{\partial t} + \frac{u}{\lambda}\frac{\partial w}{\partial x} + v\frac{\partial w}{\partial y} + \frac{w}{r}\frac{\partial w}{\partial \varphi} + \frac{1}{\rho r}\frac{\partial p}{\partial \varphi} + \frac{\cos\theta}{r}uw + \frac{\sin\theta}{r}vw\right)$$

$$+ \left\{\frac{\partial p}{\partial t} + \frac{u}{\lambda}\frac{\partial p}{\partial x} + v\frac{\partial p}{\partial y} + \frac{w}{r}\frac{\partial p}{\partial \varphi} + \rho a^2\left[\frac{1}{\lambda}\frac{\partial u}{\partial x} + \frac{\partial v}{\partial y} + \frac{\partial w}{\partial \varphi} + \frac{\cos\theta}{r}u + \left(\frac{K}{\lambda} + \frac{\sin\theta}{r}\right)v\right]\right\} = 0 \qquad \text{(C3)}$$

The quantities $\mp h_x\Big/\sqrt{h_x^2 + h_y^2 + h_\varphi^2}$, $\mp h_y\Big/\sqrt{h_x^2 + h_y^2 + h_\varphi^2}$, and $\mp h_\varphi\Big/\sqrt{h_x^2 + h_y^2 + h_\varphi^2}$ have all the properties of direction cosines. In this paper these quantities are chosen to be the same as the direction cosines of the shock normal, $\cos\beta_x$, $\cos\beta_y$, and $\cos\beta_\varphi$, so that the total derivatives dp/dt and dV/dt will appear in the compatibility relation which is used and dU/dt will not. It has been assumed that the bicharacteristic can be approximated by a straight line so that the quantities h_t, h_x, h_y, and h_φ can be considered constant. With these assumptions, the compatibility relation can be written as

$$\frac{\partial p}{\partial t} + \frac{1}{\lambda}\left(u + a\cos\beta_x\right)\frac{\partial p}{\partial x} + \left(v + a\cos\beta_y\right)\frac{\partial p}{\partial y} + \frac{1}{r}\left(w + a\cos\beta_\varphi\right)\frac{\partial p}{\partial \varphi} + \rho a\left(\frac{\partial V}{\partial t} + \frac{u}{\lambda}\frac{\partial V}{\partial x} + v\frac{\partial V}{\partial y}\right.$$

$$\left. + \frac{w}{r}\frac{\partial V}{\partial \varphi}\right) + \rho a^2\left(\frac{1}{\lambda}\frac{\partial u}{\partial x} + \frac{\partial v}{\partial y} + \frac{1}{r}\frac{\partial w}{\partial \varphi}\right) = -\frac{\rho a}{\lambda}\left(av - u^2\cos\beta_y + uv\cos\beta_x\right)v - \frac{\rho a}{r}\left[\left(av - w^2\cos\beta_y\right.\right.$$

$$\left.\left. + vw\cos\beta_\varphi\right)\sin\theta + \left(au - w^2\cos\beta_x + uw\cos\beta_\varphi\right)\cos\theta\right]$$

(C4)

APPENDIX C

With the aid of equations (29) and (34), it can be shown that the following relationship holds:

$$\frac{1}{\lambda}\frac{\partial u}{\partial x} + \frac{\partial v}{\partial y} + \frac{1}{r}\frac{\partial w}{\partial \varphi} = \frac{\cos \beta_x}{\lambda}\frac{\partial V}{\partial x} + \cos \beta_y \frac{\partial V}{\partial y} + \frac{\cos \beta_\varphi}{r}\frac{\partial V}{\partial \varphi} + \frac{1}{\lambda}\frac{\partial U_x}{\partial x} + \frac{\partial U_y}{\partial y} + \frac{1}{r}\frac{\partial U_\varphi}{\partial \varphi} \qquad (C5)$$

Equations (C4) and (C5) can be combined to yield

$$\left(\frac{dp}{dt}\right)_+ + \rho a\left(\frac{dV}{dt}\right)_+ = -\rho a^2\left(\frac{1}{\lambda}\frac{\partial U_x}{\partial x} + \frac{\partial U_y}{\partial y} + \frac{1}{r}\frac{\partial U_\varphi}{\partial \varphi}\right) - \frac{\rho a}{\lambda}\left(av - u^2\cos \beta_y + uv \cos \beta_x\right)K$$

$$- \frac{\rho a}{r}\left[\left(av - w^2\cos \beta_y + vw \cos \beta_\varphi\right)\sin \theta\right.$$

$$\left. + \left(au - w^2\cos \beta_x + uw \cos \beta_\varphi\right)\cos \theta\right] \qquad (C6)$$

where $(d/dt)_+$ denotes the total time derivative along the bicharacteristic and is written as

$$\left(\frac{d}{dt}\right)_+ = \frac{\partial}{dt} + \frac{1}{\lambda}\left(u + a \cos \beta_x\right)\frac{\partial}{\partial x} + \left(v + a \cos \beta_y\right)\frac{\partial}{\partial y} + \frac{1}{r}\left(w + a \cos \beta_\varphi\right)\frac{\partial}{\partial \varphi} \qquad (C7)$$

The bicharacteristic has the slopes

$$\left(\frac{dx}{dt}\right)_+ = \frac{1}{\lambda}\left(u + a \cos \beta_x\right) \qquad \left(\frac{dy}{dt}\right)_+ = \left(v + a \cos \beta_y\right) \qquad \left(\frac{d\varphi}{dt}\right)_+ = \frac{1}{r}\left(w + a \cos \beta_\varphi\right)$$

For the purposes of the paper, it is desired to express the compatibility relation in terms of the independent variables τ, X, Y, and Φ which are given by equations (7). This is accomplished with the aid of expressions (8) which relate the partial derivatives with respect to t, x, y, and φ to those with respect to τ, X, Y, and Φ. First consider the first group of terms on the right side of equation (C6). These terms can be transformed as follows:

APPENDIX C

$$\frac{1}{\lambda}\frac{\partial U_x}{\partial x}+\frac{\partial U_y}{\partial y}+\frac{1}{r}\frac{\partial U_\varphi}{\partial \varphi}=\frac{1}{\lambda}\frac{\partial U_x}{\partial X}-\frac{1}{\lambda\delta}\left(\delta'+y_b'\right)\frac{\partial U_x}{\partial Y}+\frac{1}{\delta}\frac{\partial U_y}{\partial Y}+\frac{1}{r}\frac{\partial U_\varphi}{\partial \Phi}-\frac{1}{r\delta}\left(\hat{\delta}+\hat{y}_b\right)\frac{\partial U_\varphi}{\partial Y}$$

$$=\frac{1}{\lambda}\frac{\partial U_x}{\partial X}+\frac{G}{\delta}\left(\cos\beta_x\frac{\partial U_x}{\partial Y}+\cos\beta_y\frac{\partial U_y}{\partial Y}+\cos\beta_\varphi\frac{\partial U_\varphi}{\partial Y}\right)+\frac{1}{r}\frac{\partial U_\varphi}{\partial \Phi}$$

$$=\frac{1}{\lambda}\frac{\partial U_x}{\partial X}+\frac{G}{\delta}\frac{\partial}{\partial Y}\left(\vec{e}_s\cdot\vec{U}\right)+\frac{1}{r}\frac{\partial U_\varphi}{\partial \Phi}$$

$$=\frac{1}{\lambda}\frac{\partial U_x}{\partial X}+\frac{1}{r}\frac{\partial U_\varphi}{\partial \Phi}$$

The last step follows because

$$\vec{e}_s\cdot\vec{U}=0$$

Similarly, the expression (C7) for the total derivative with respect to time along the bicharacteristic can be transformed as follows:

$$\left(\frac{d}{dt}\right)_+=\frac{\partial}{\partial\tau}-\frac{\dot{\delta}}{\delta}\frac{\partial}{\partial Y}+\frac{1}{\lambda}\left(u+a\cos\beta_x\right)\left[\frac{\partial}{\partial X}-\frac{1}{\delta}\left(\delta'+y_b'\right)\frac{\partial}{\partial Y}\right]+\frac{1}{\delta}\left(v+a\cos\beta_y\right)\frac{\partial}{\partial Y}$$

$$+\frac{1}{r}\left(w+a\cos\beta_\varphi\right)\left[\frac{\partial}{\partial\Phi}-\frac{1}{\delta}\left(\hat{\delta}+\hat{y}_b\right)\frac{\partial}{\partial Y}\right]$$

$$=\frac{\partial}{\partial\tau}+\frac{1}{\lambda}\left(u+a\cos\beta_x\right)\frac{\partial}{\partial X}+\frac{1}{\delta}\left[G(V+a)-\dot{\delta}\right]\frac{\partial}{\partial Y}+\frac{1}{r}\left(w+a\cos\beta_\varphi\right)\frac{\partial}{\partial\Phi}$$

Thus, the compatibility relation can be written in terms of the independent variables τ, X, Y, and Φ as

$$\frac{\partial p}{\partial\tau}+\frac{1}{\lambda}\left(u+a\cos\beta_x\right)\frac{\partial p}{\partial X}+\frac{1}{\delta}\left[G(V+a)-\dot{\delta}\right]\frac{\partial p}{\partial Y}+\frac{1}{r}\left(w+a\cos\beta_\varphi\right)\frac{\partial p}{\partial\Phi}+\rho a\left\{\frac{\partial V}{\partial\tau}+\frac{1}{\lambda}\left(u+a\cos\beta_x\right)\frac{\partial V}{\partial X}\right.$$

$$\left.+\frac{1}{\delta}\left[G(V+a)-\dot{\delta}\right]\frac{\partial V}{\partial Y}+\frac{1}{r}\left(w+a\cos\beta_\varphi\right)\frac{\partial V}{\partial\Phi}\right\}=-\rho a\left[a\left(\frac{1}{\lambda}\frac{\partial U_x}{\partial X}+\frac{1}{r}\frac{\partial U_\varphi}{\partial\Phi}\right)+\frac{K}{\lambda}\left(av-u^2\cos\beta_y\right.\right.$$

$$\left.+uv\cos\beta_x\right)+\frac{\sin\theta}{r}\left(av-w^2\cos\beta_y+vw\cos\beta_\varphi\right)$$

$$\left.+\frac{\cos\theta}{r}\left(au-w^2\cos\beta_x+uw\cos\beta_\varphi\right)\right]$$

REFERENCES

1. Rusanov, V. V.: Three-Dimensional Flow About an Arbitrary Blunt Body. Aerospace Proceedings 1966, Vol. 1, Joan Bradbrooke, Joan Bruce, and Robert R. Dexter, eds., Macmillan Co., 1966, pp. 291-301.

2. Bohachevsky, Ihor O.; and Mates, Robert E.: A Direct Method for Calculation of the Flow About an Axisymmetric Blunt Body at Angle of Attack. AIAA J., vol. 4, no. 5, May 1966, pp. 776-782.

3. Moretti, Gino; and Bleich, Gary: Three-Dimensional Flow Around Blunt Bodies. AIAA J., vol. 5, no. 9, Sept. 1967, pp. 1557-1562.

4. Xerikos, J.; and Anderson, W. A.: A Time-Dependent Approach to the Numerical Solution of the Flow Field About an Axisymmetric Vehicle at Angle of Attack. DAC-62279 (Contract NAS 8-21141), Douglas Aircraft Co., June 1968. (Available as NASA CR-61982.)

5. Cohen, Gerald A.; Foster, Richard M.; and Dowty, James R.: Synthesis of Optimum Structural Designs for Conical and Tension Shell Mars Entry Capsules. NASA CR-1365, 1969.

6. Masson, B. S.; Taylor, T. D.; and Foster, R. M.: Application of Godunov's Method to Blunt-Body Calculations. AIAA J., vol. 7, no. 4, Apr. 1969, pp. 694-698.

7. Barnwell, R. W.: Three-Dimensional Flow Around Blunt Bodies With Sharp Shoulders. AIAA Paper No. 71-56, Jan. 1971.

8. Barnwell, Richard W.: Time-Dependent Numerical Method for Treating Complicated Blunt-Body Flow Fields. Analytical Methods in Aircraft Aerodynamics, NASA SP-228, 1970, pp. 177-195.

9. Barnwell, Richard W.: A Time-Dependent Method for Calculating Supersonic Blunt-Body Flow Fields With Sharp Corners and Embedded Shock Waves. NASA TN D-6031, 1970.

10. Moretti, Gino; and Abbett, Michael: A Time-Dependent Computational Method for Blunt Body Flows. AIAA J., vol. 4, no. 12, Dec. 1966, pp. 2136-2141.

11. Brailovskaya, I. Yu.: A Difference Scheme for Numerical Solution of the Two-Dimensional, Nonstationary Navier-Stokes Equations for a Compressible Gas. Sov. Phys. – Doklady, vol. 10, no. 2, Aug. 1965, pp. 107-110.

12. Richtmyer, R. D.; and Morton, K. W.: Stability Studies With Difference Equations. (I) Non-Linear Stability. (II) Coupled Sound and Heat Flow. NYO-1480-5 (Contract AT(30-1)-1480), Courant Inst. Math. Sci., New York Univ., Aug. 25, 1964.

13. Barnwell, Richard W.: Inviscid Radiating Shock Layers About Spheres Traveling at Hyperbolic Speeds in Air. NASA TR R-311, 1969.

14. Guderley, K. Gottfried: Singularities at the Sonic Velocity. Tech. Rep. No. F-TR-1171-ND, Air Materiel Command, U.S. Air Force, June 1948.

15. Friedman, Manfred P.: Two-Dimensional and Axisymmetric Rotational Flows Past a Transonic Corner. J. Aerosp. Sci., vol. 29, no. 4, Apr. 1962, pp. 503-504.

16. Shifrin, E. G.: On the Extremal Properties of Entropy on a Critical Streamline. J. Appl. Math. Mech., vol. 31, no. 3, 1967, pp. 618-620.

17. Webb, H. G., Jr.; Dresser, H. S.; Adler, B. K.; and Waiter, S. A.: Inverse Solution of Blunt-Body Flowfields at Large Angle of Attack. AIAA J., vol. 5, no. 6, June 1967, pp. 1079-1085.

18. Anon.: U.S. Standard Atmosphere, 1962. NASA, U.S. Air Force, and U.S. Weather Bur., Dec. 1962.

19. Kendall, James M., Jr.: Experiments on Supersonic Blunt-Body Flows. Progr. Rep. No. 20-372 (Contract No. DA-04-495-Ord 18), Jet Propulsion Lab., California Inst. Technol., Feb. 27, 1959.

20. Stallings, Robert L., Jr.; and Howell, Dorothy T.: Experimental Pressure Distributions for a Family of Blunt Bodies at Mach Numbers From 2.49 to 4.63 and Angles of Attack From 0° to 15°. NASA TN D-5392, 1969.

21. Stallings, Robert L., Jr.; and Tudor, Dorothy H.: Experimental Pressure Distributions on a 120° Cone at Mach Numbers From 2.96 to 4.63 and Angles of Attack From 0° to 20°. NASA TN D-5054, 1969.

22. Allison, Dennis O.: Calculation of Thermodynamic Properties of Gas Mixtures at High Temperatures. M.S. Thesis, Virginia Polytech. Inst., 1965.

23. Browne, W. G.: Thermodynamic Properties of the Earth's Atmosphere. Radiation and Space Phys. Tech. Mem. No. 2, Missile Space Div., Gen. Elec. Co., Nov. 15, 1962.

24. Richtmyer, Robert D.: A Survey of Difference Methods for Non-Steady Fluid Dynamics. NCAR Tech. Notes 63-2, Nat. Center Atmos. Res., Aug. 27, 1962.

25. Van Leer, B.: Stabilization of Difference Schemes for the Equations of Inviscid Compressible Flow by Artificial Diffusion. J. Comput. Phys., vol. 3, no. 4, Apr. 1969. pp. 473-485.

26. Von Mises, Richard: Mathematical Theory of Compressible Fluid Flow. Academic Press, Inc., 1958, pp. 100-116.

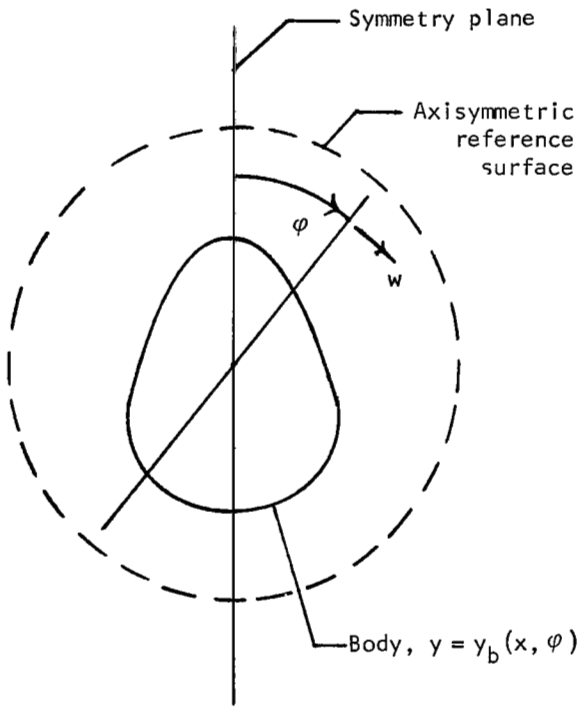

(a) Front view.

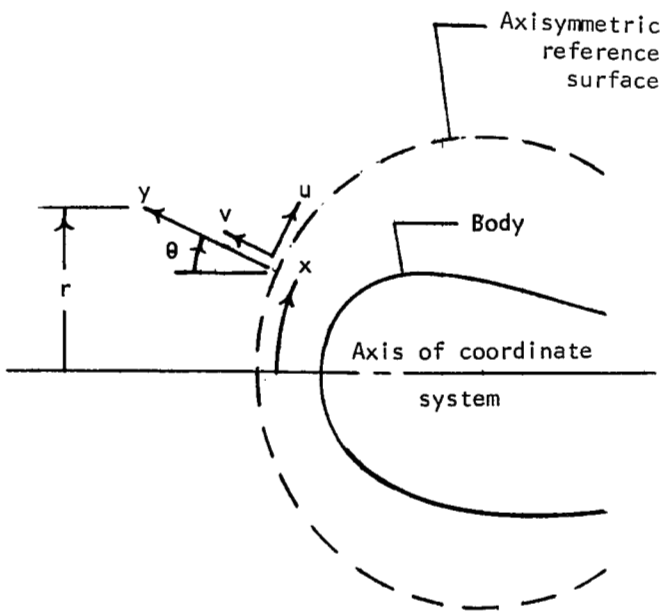

(b) Representative φ-plane.

Figure 1.- Basic coordinate system.

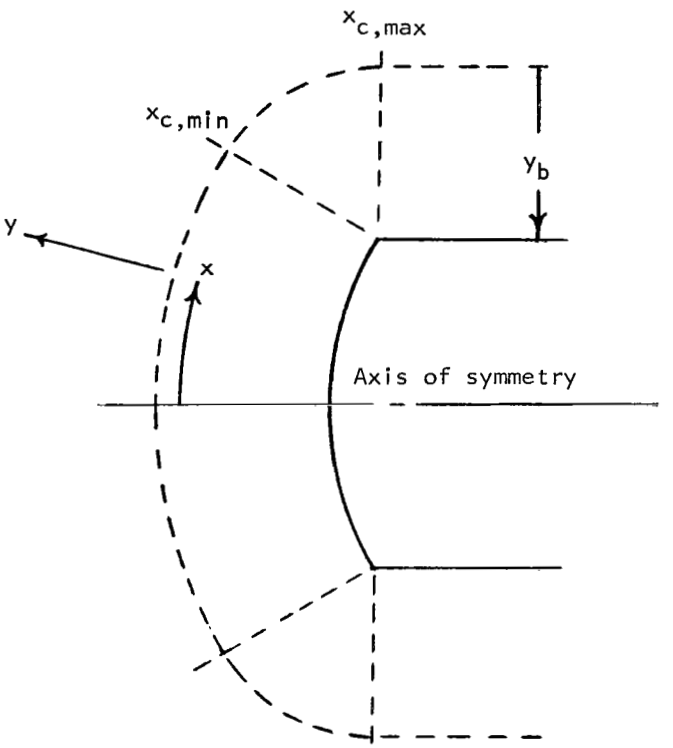

Figure 2.- Coordinate system for sharp-shouldered body.

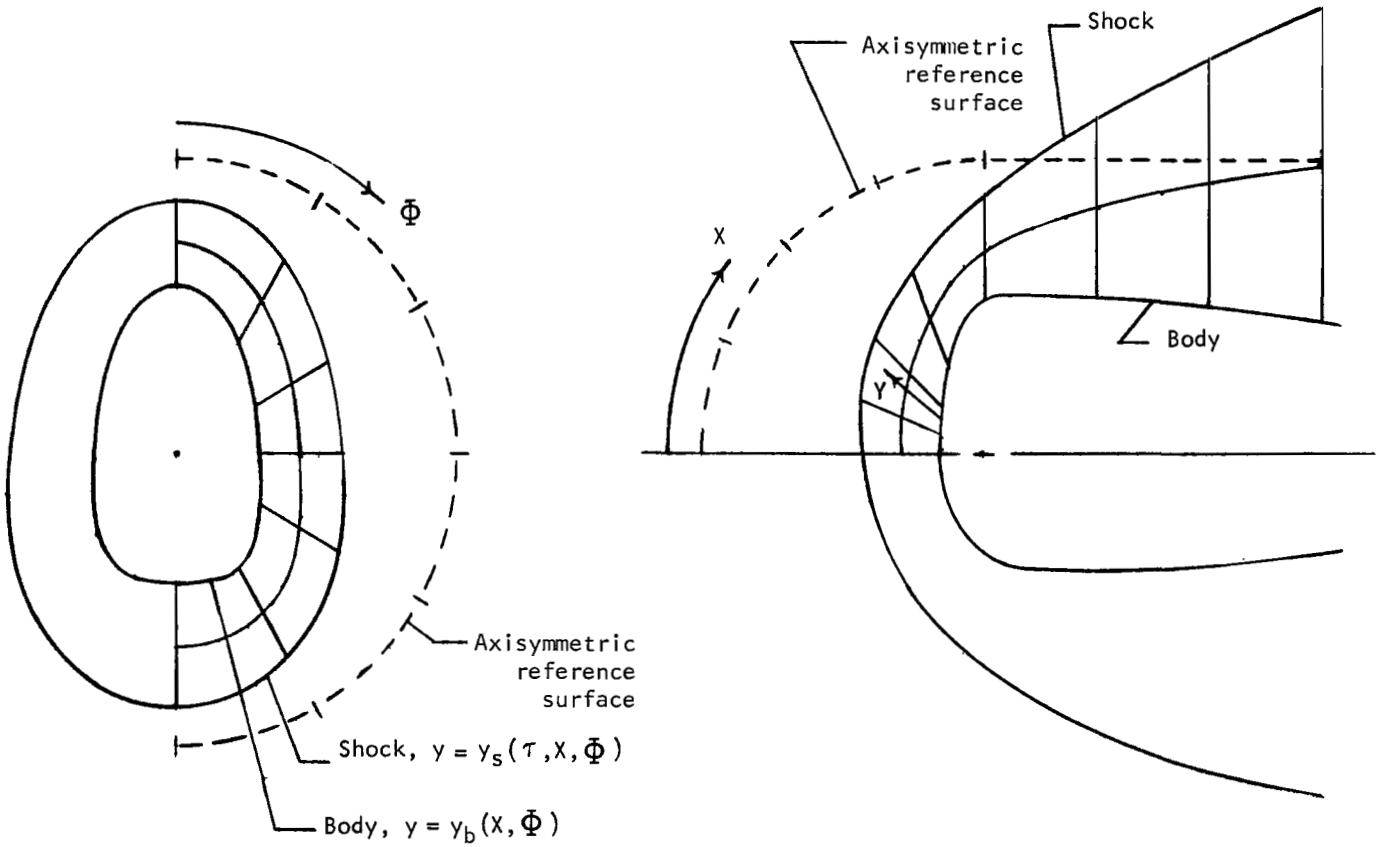

(a) Front view.

(b) Representative Φ-plane.

Figure 3.- Computational grid.

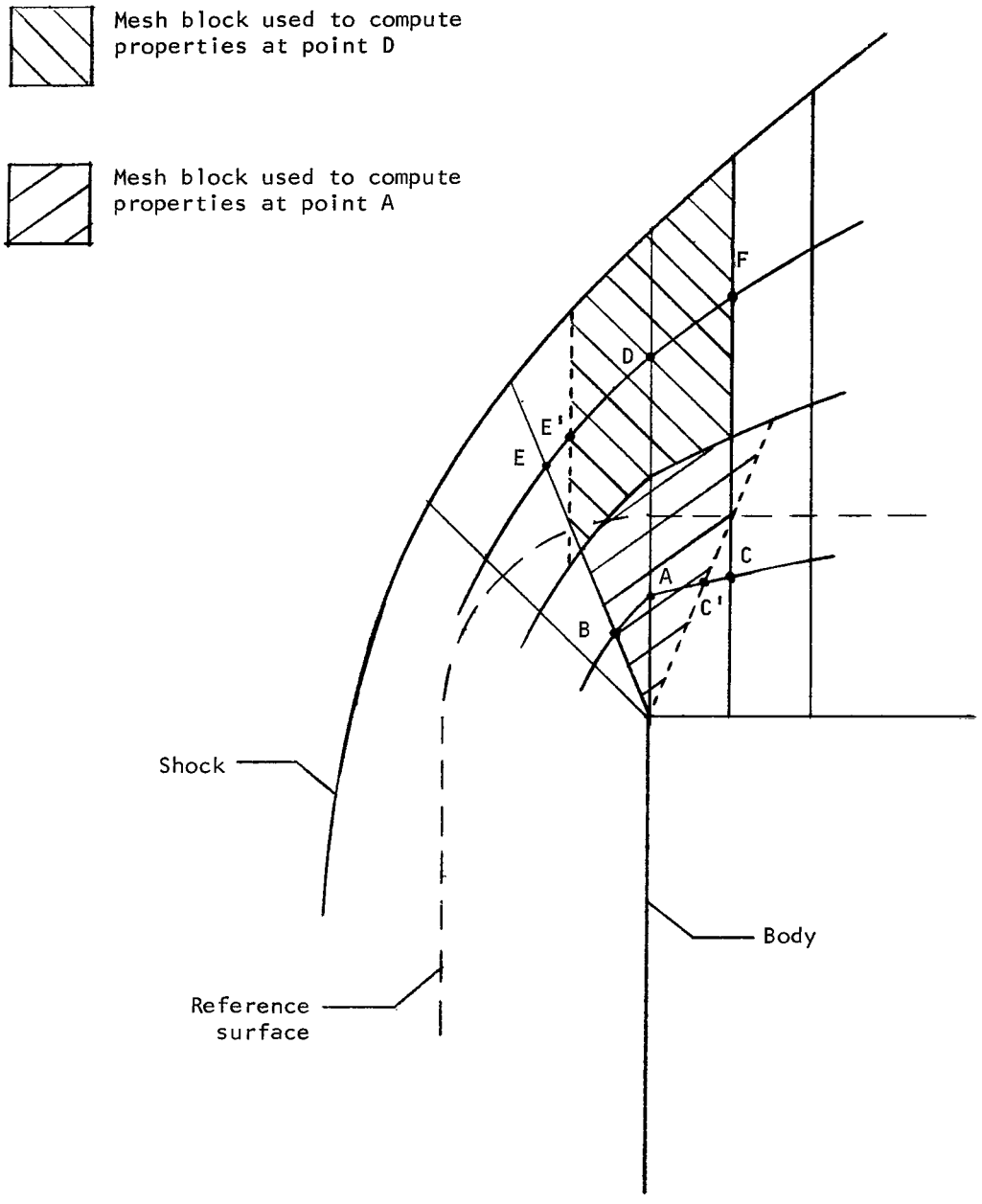

Figure 4.- Computational grid for points where curvature changes.

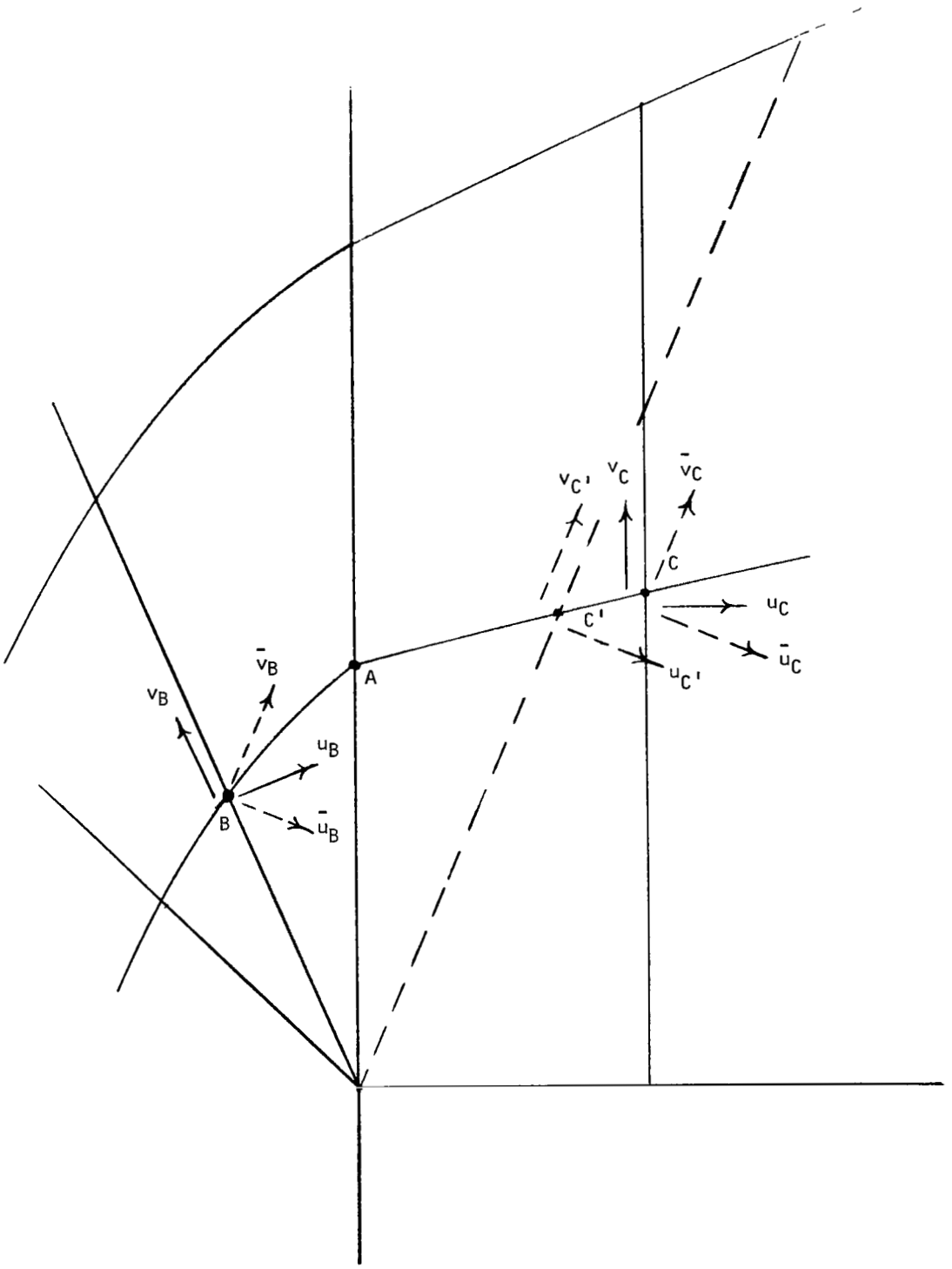

Figure 5.- Interpolation of flow properties at point C'.

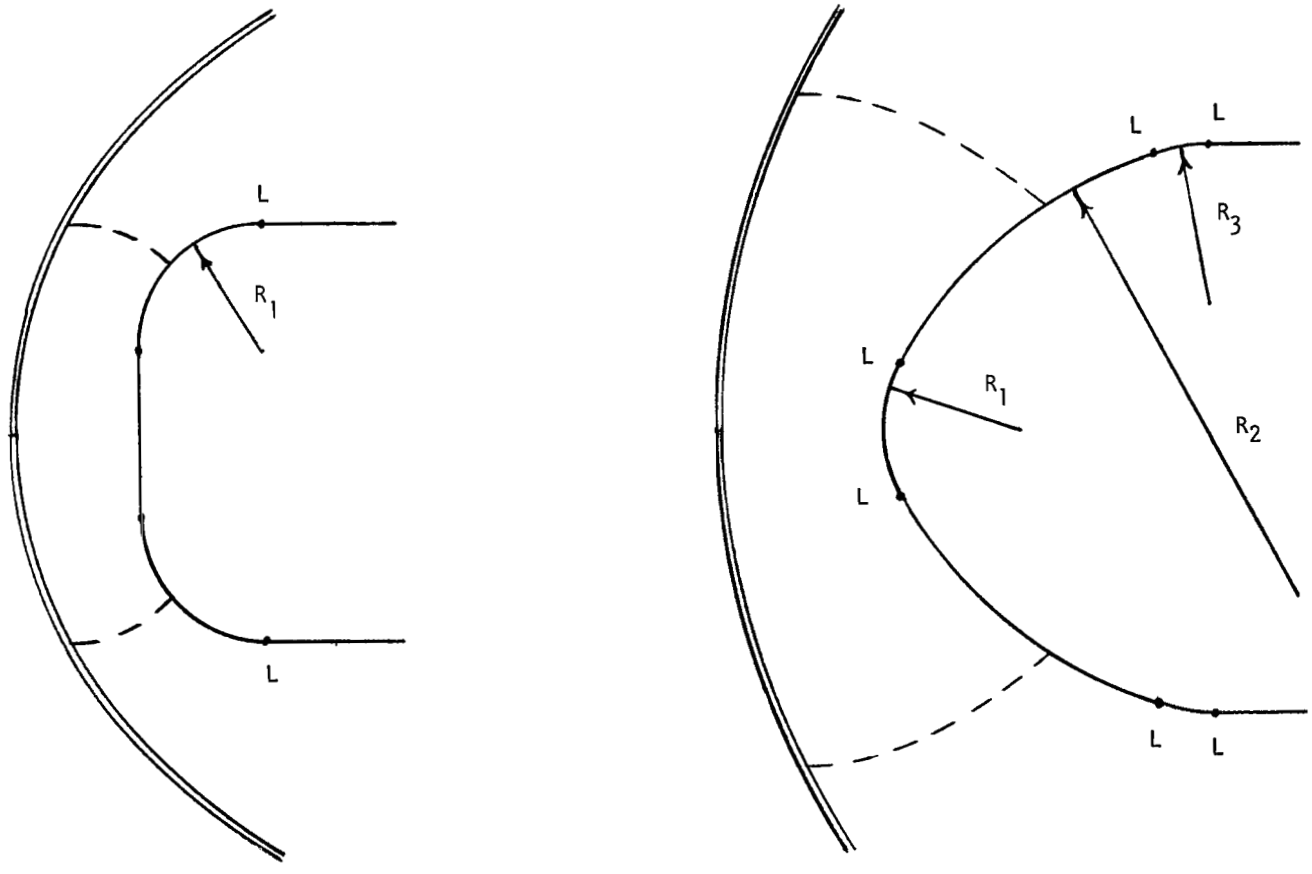

Shock

Sonic line

L Junction where flow property derivatives tend to be large

R_1, R_2, R_3 Radii of curvature of segments of body surface generator

Figure 6.- Examples of bodies with junctions where curvature is large.

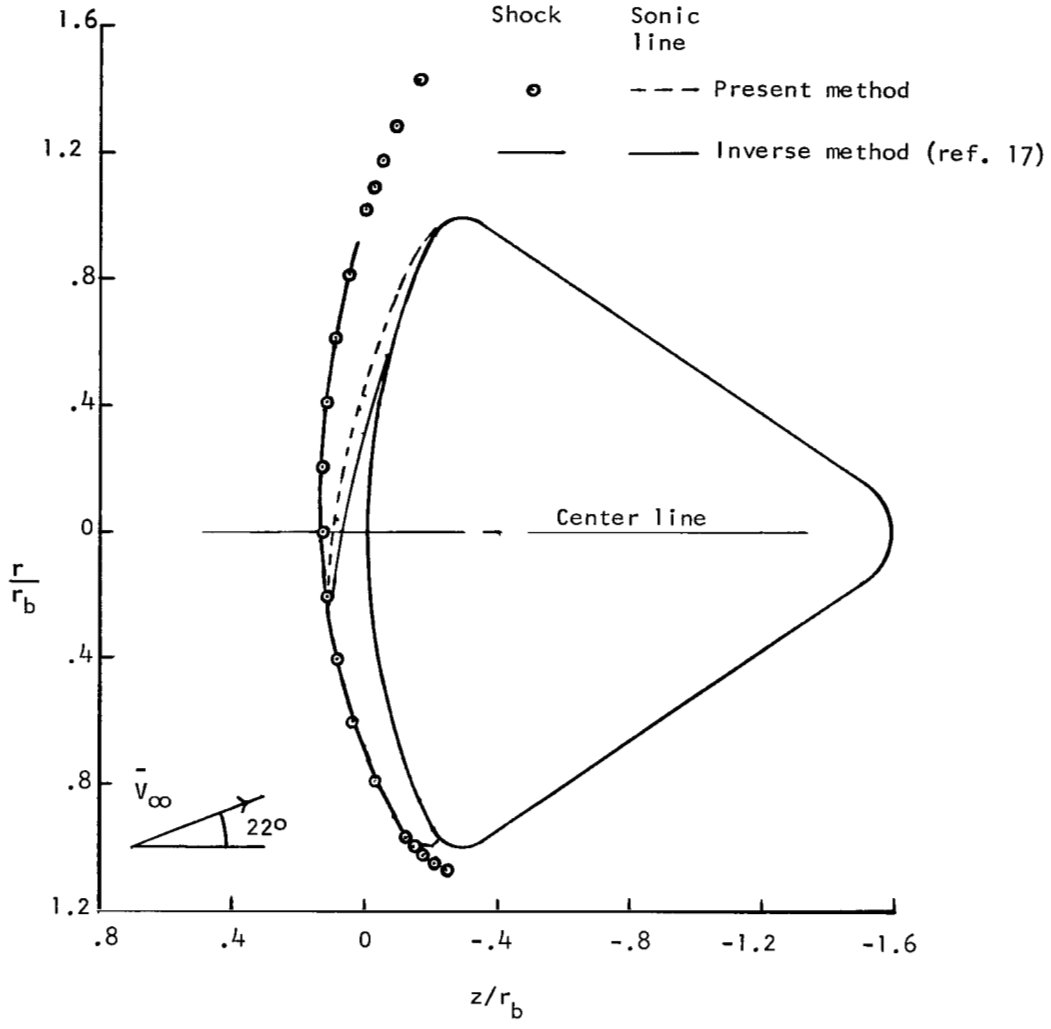

(a) Bow-shock-wave and sonic-line locations in plane of symmetry.

Figure 7.- Comparison of results for equilibrium air flow field about Apollo command module at 22° angle of attack and traveling at a speed of 6935 m/s (22 754 ft/sec) at an altitude of 45.866 km (150 480 ft).

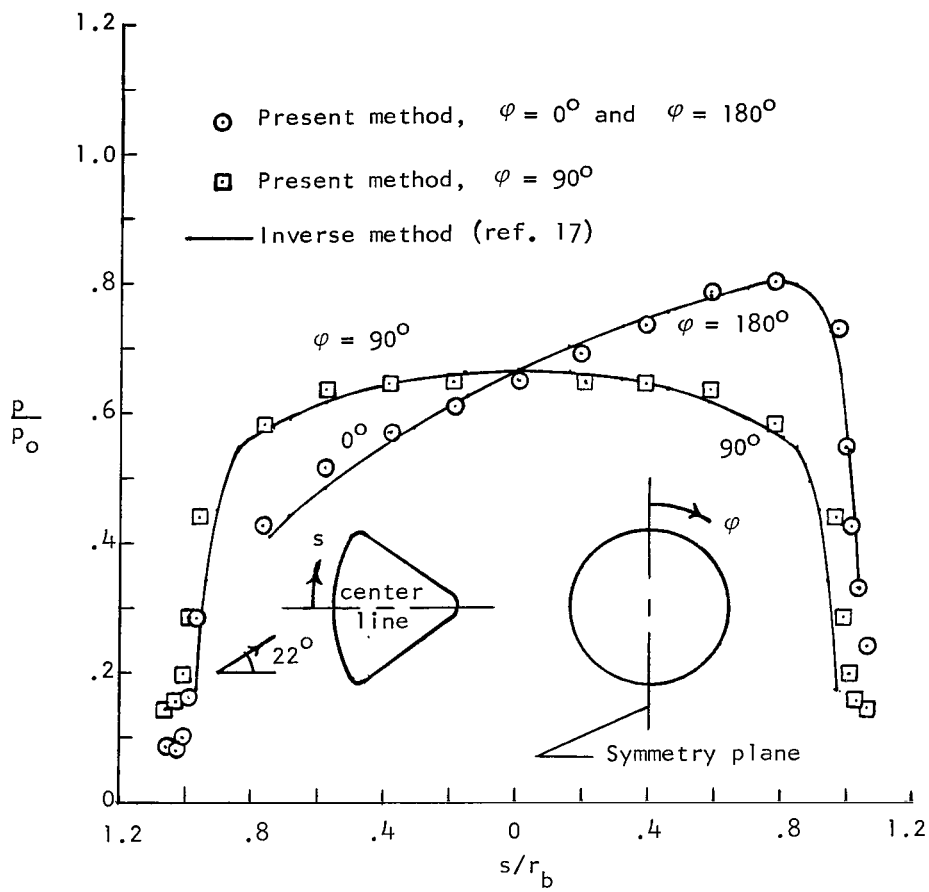

(b) Surface pressure distribution for plane of symmetry ($\varphi = 0^{o}$ and 180^{o}) and plane normal to plane of symmetry ($\varphi = 90^{o}$).

Figure 7.- Concluded.

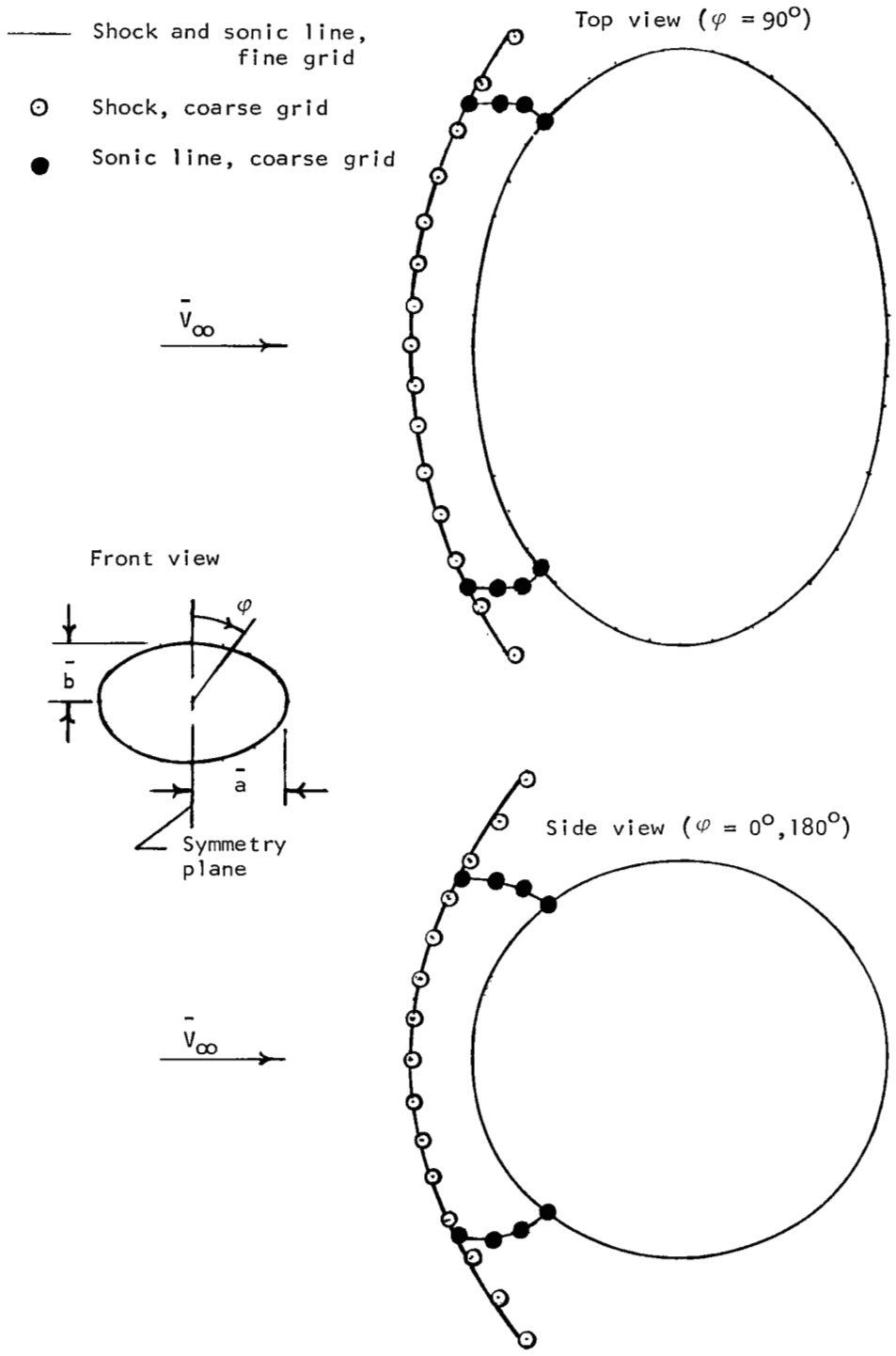

(a) Shock-wave and sonic-line shapes for planes of symmetry.

Figure 8.- Flow field about prolate spheroid with $\bar{a}/\bar{b} = 3/2$ and with its axis normal to the direction of flow for $M_{\infty} = 3$ and $\gamma = 1.4$.

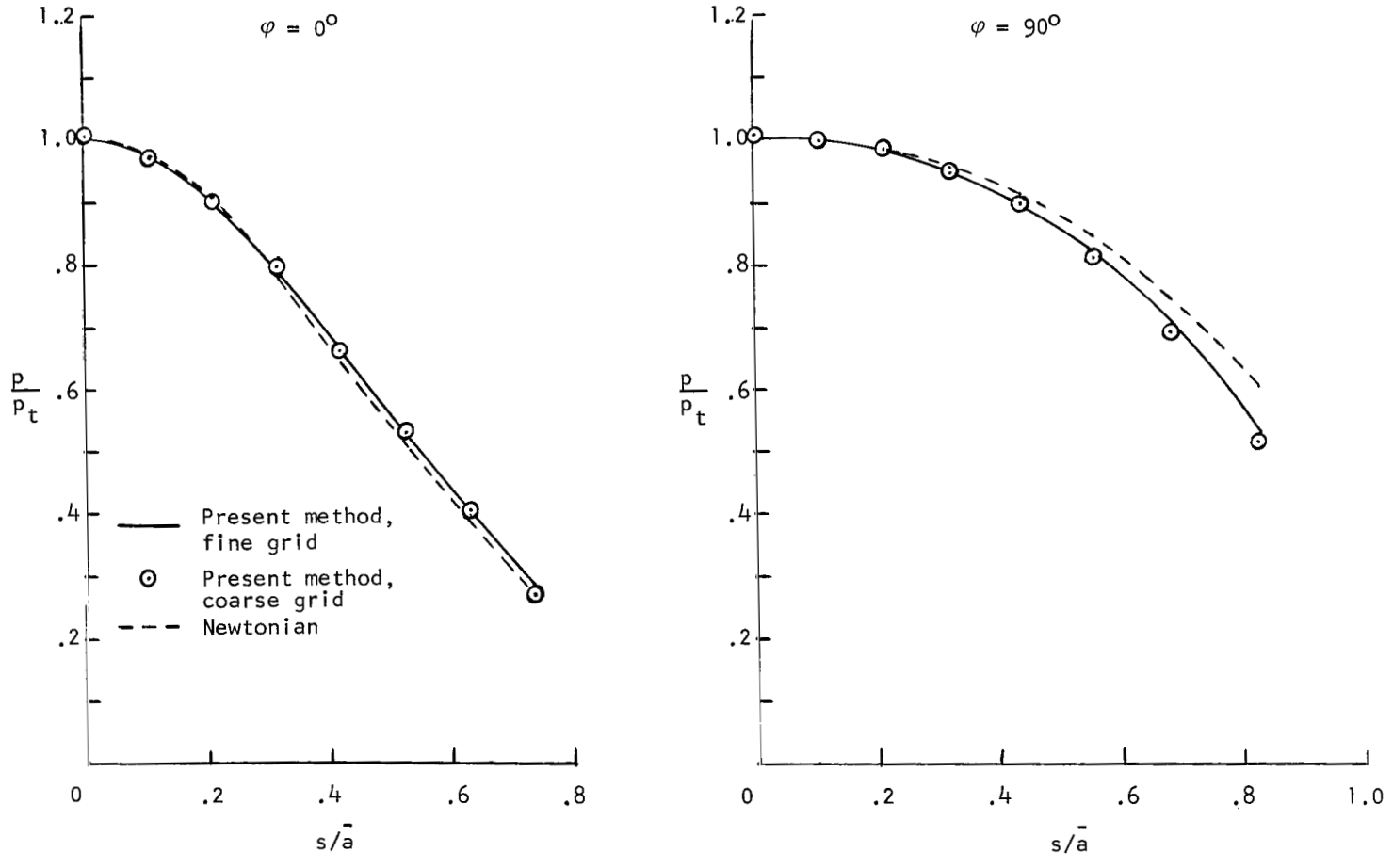

(b) Surface pressure distributions in planes of symmetry.

Figure 8.- Concluded.

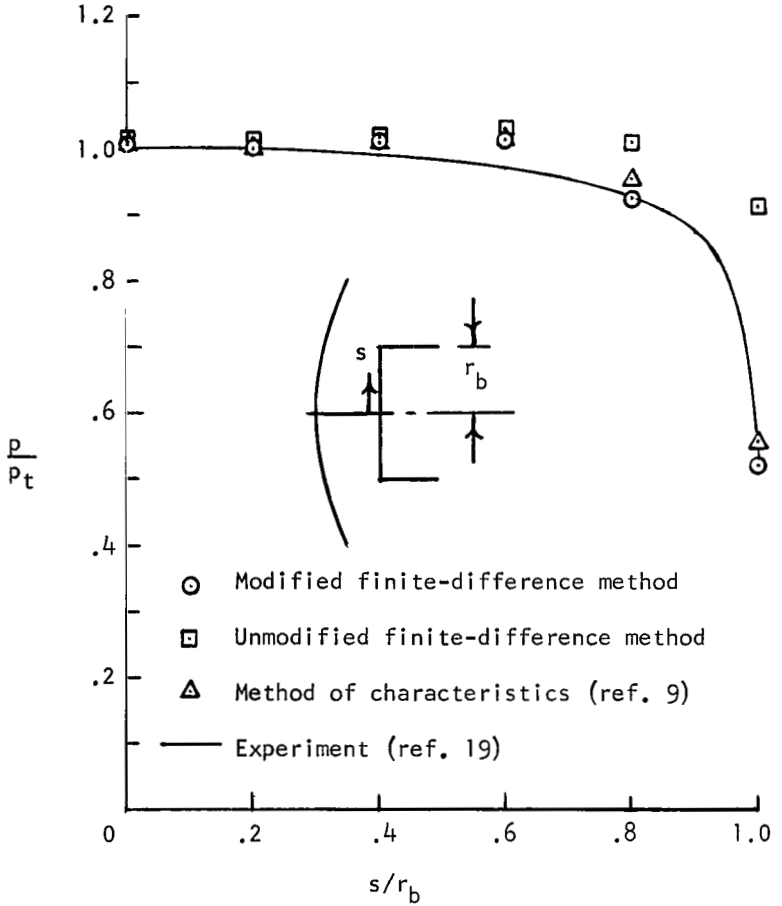

(a) Surface pressure distribution.

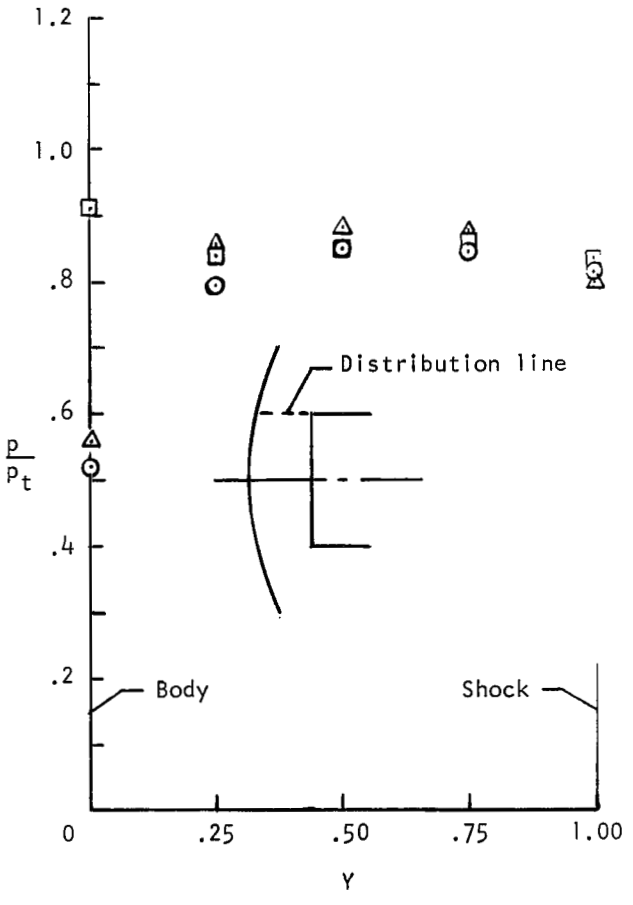

(b) Pressure distribution across shock at shoulder along line shown.

Figure 9.- Pressure distribution on surface and along line across shock layer at shoulder for flat-face cylinder at 0^{o} angle of attack with $M_{\infty} = 2.81$ and $\gamma = 1.4$.

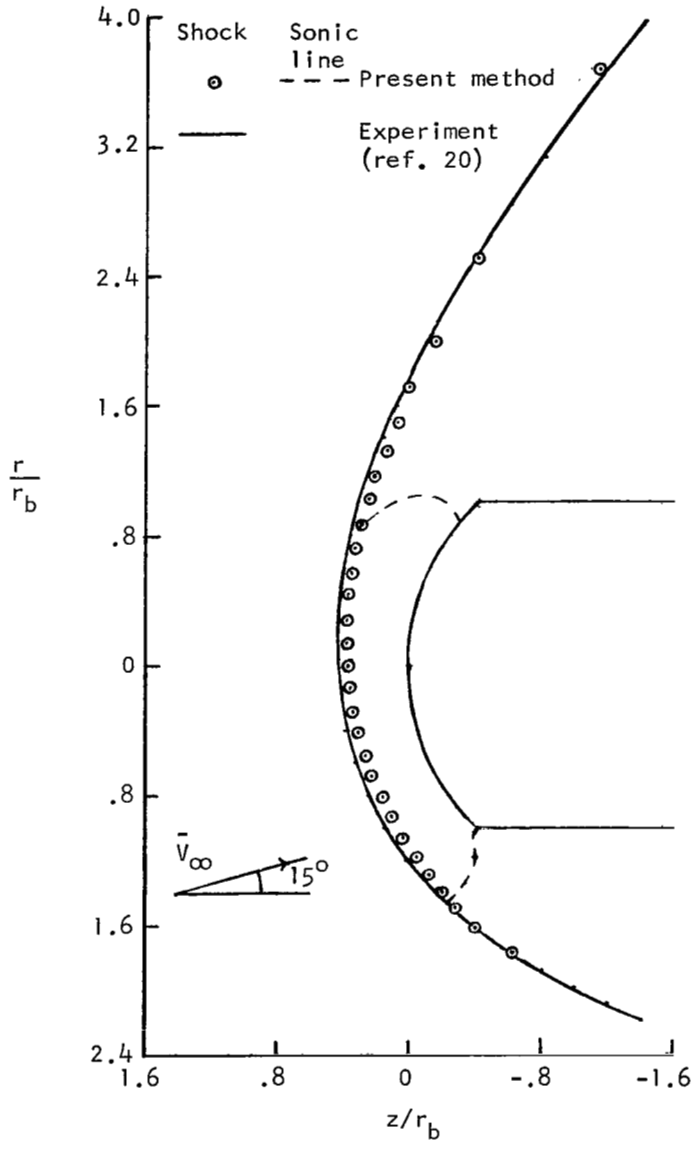

(a) Shock-wave and sonic-line locations.

Figure 10.- Flow field about spherical cap with sharp shoulder at 15° angle of attack with $M_\infty = 2.49$ and $\gamma = 1.4$.

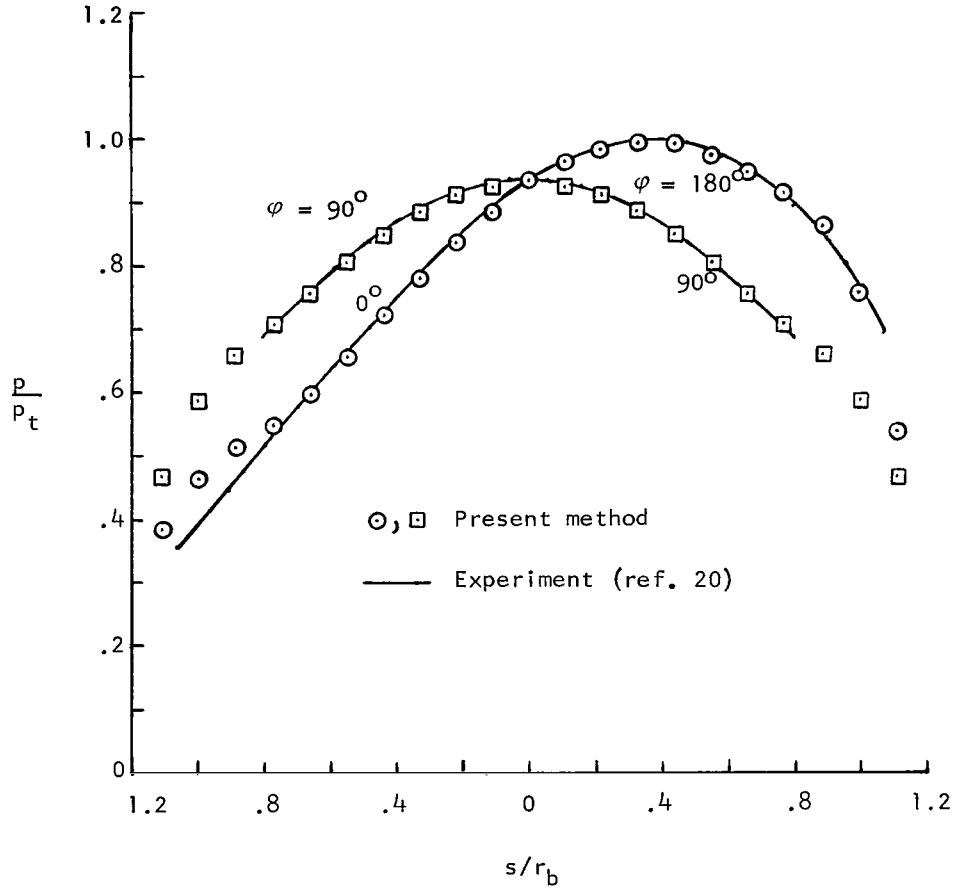

(b) Surface pressure distribution.

Figure 10.- Continued.

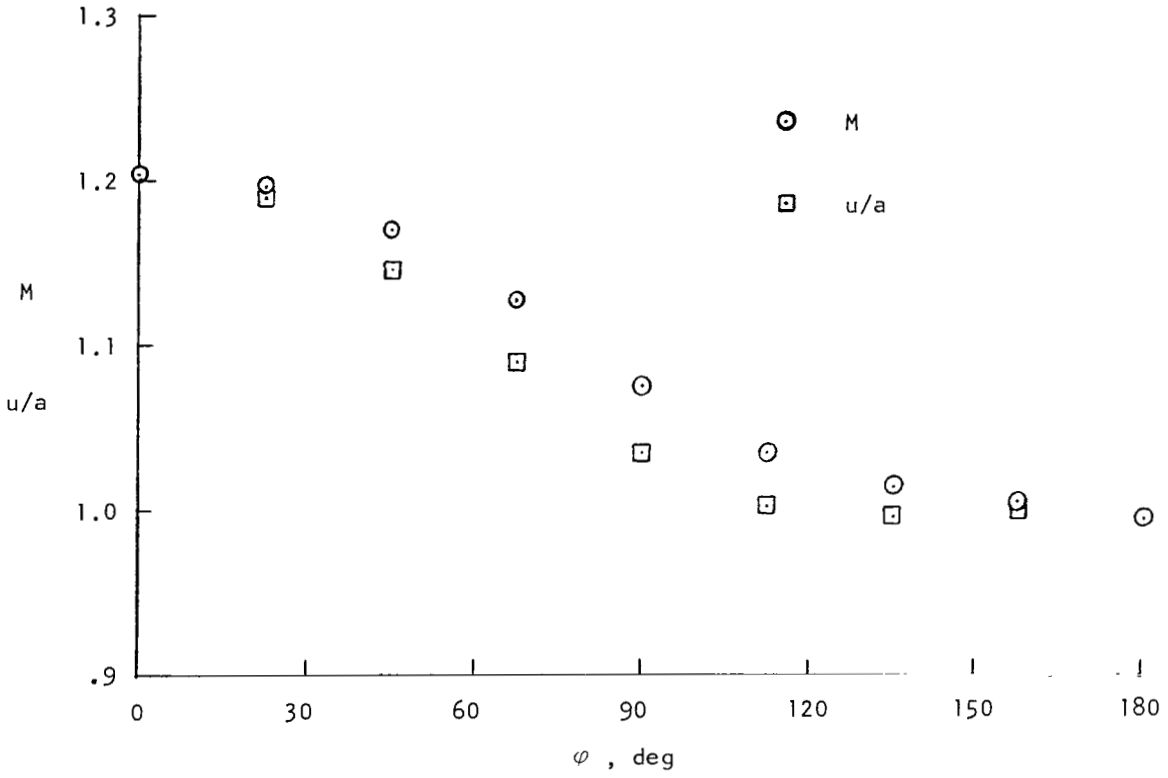

(c) Results of present method for distributions of Mach number and ratio u/a along edge.

Figure 10.- Concluded.

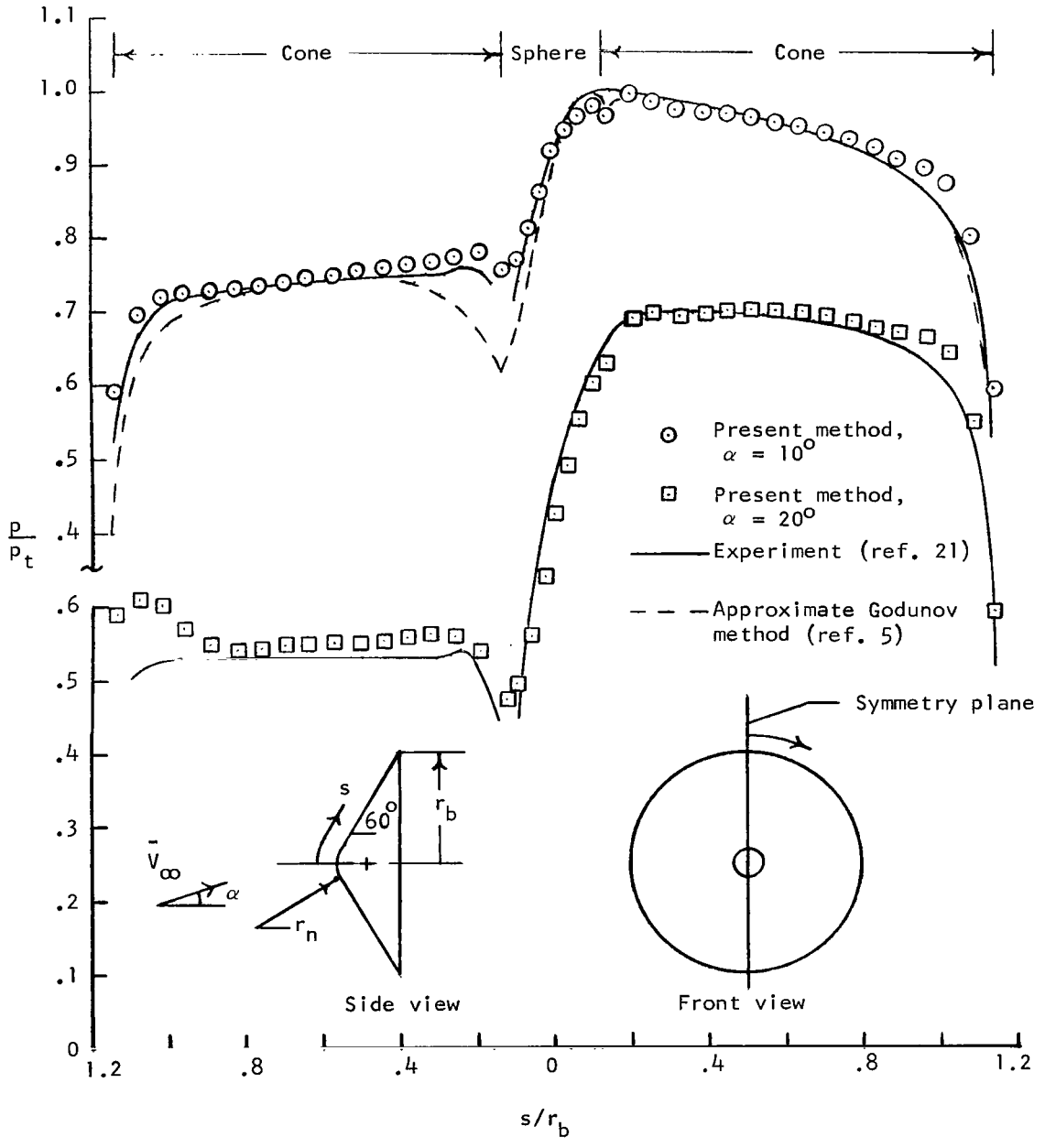

(a) Surface pressure distribution in plane of symmetry.

Figure 11.- Flow field about spherically blunted cone with sharp shoulder, semiapex angle of 60°, and ratio of nose radius to base radius of 0.25 for angles of attack of 10° and 20°. $M_\infty = 4.63$; $\gamma = 1.4$.

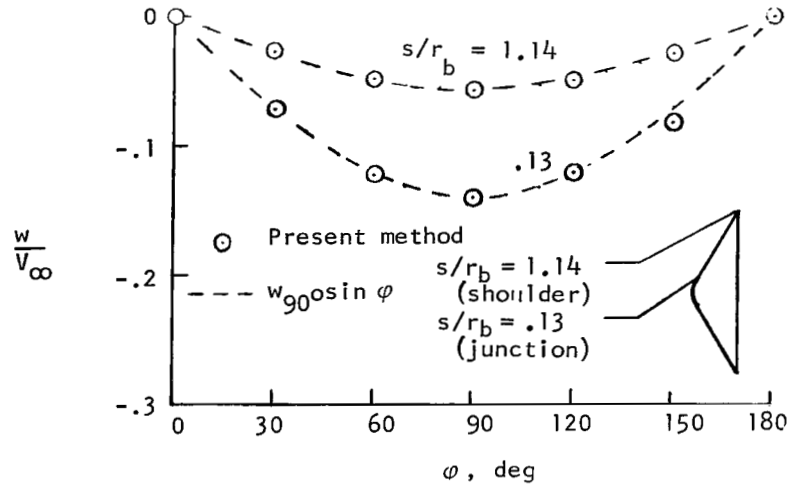

(b) Peripheral distribution of cross-flow component of velocity w for $\alpha = 10^o$.

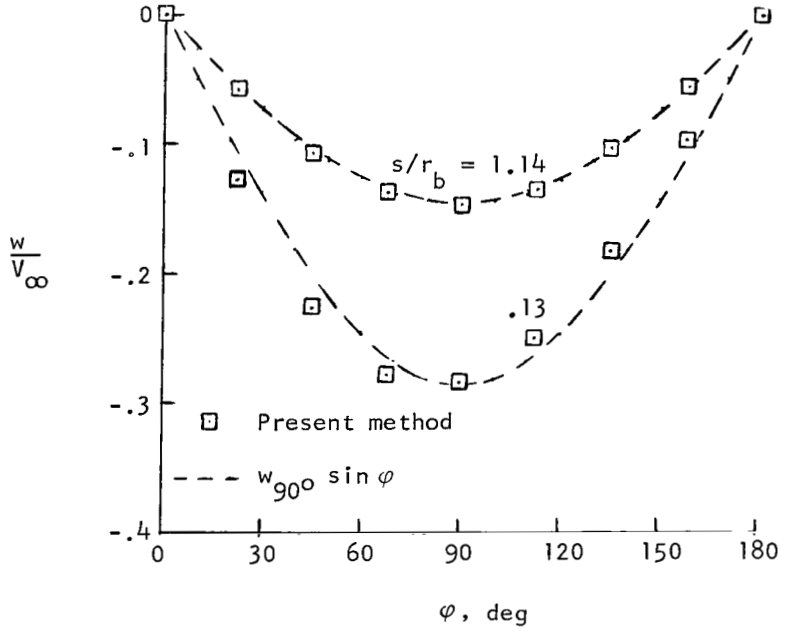

(c) Peripheral distribution of cross-flow component of velocity w for $\alpha = 20^o$.

Figure 11.- Continued.

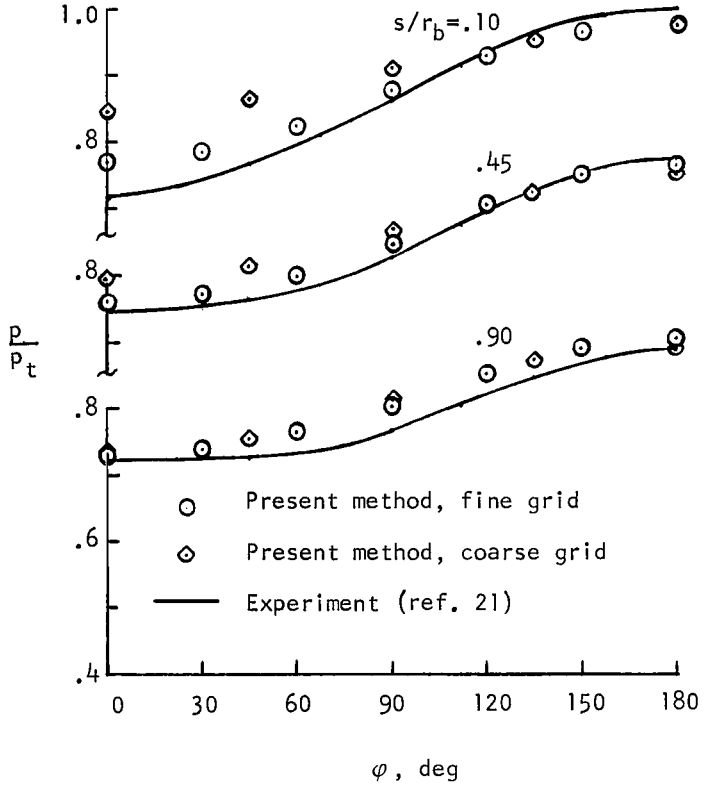

(d) Peripheral pressure distributions for $\alpha = 10^{o}$.

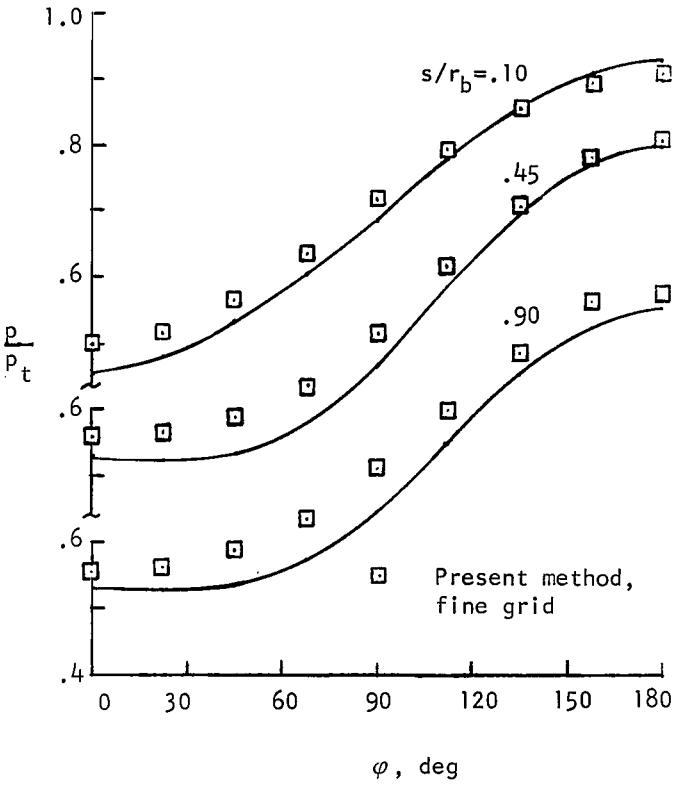

(e) Peripheral pressure distributions for $\alpha = 20^{o}$.

Figure 11.- Continued.

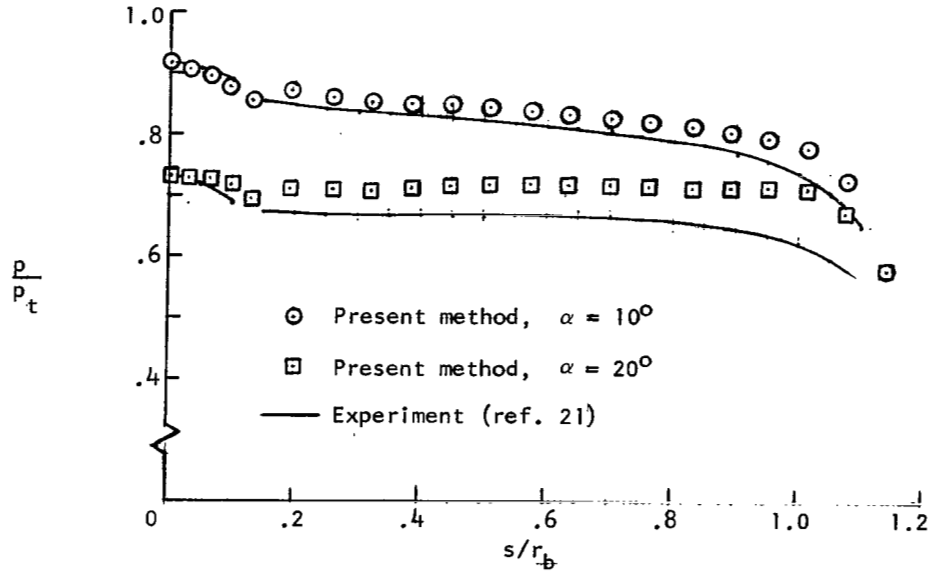

(f) Surface pressure distribution in plane $\varphi = 90^{\circ}$.

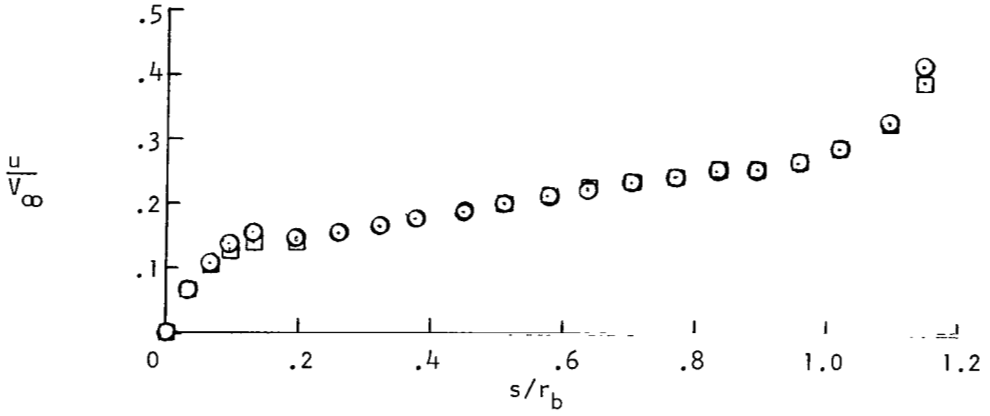

(g) Surface distribution of u-component of velocity in plane $\varphi = 90^{\circ}$.

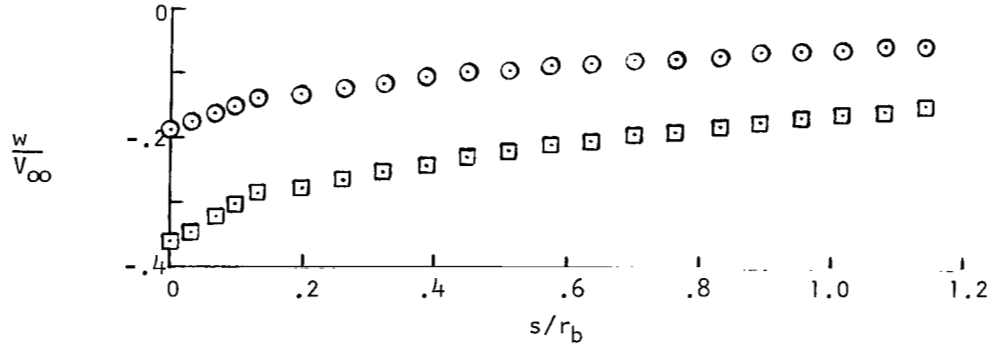

(h) Surface distribution of cross-flow component of velocity w in plane $\varphi = 90^{\circ}$

Figure 11.- Concluded.

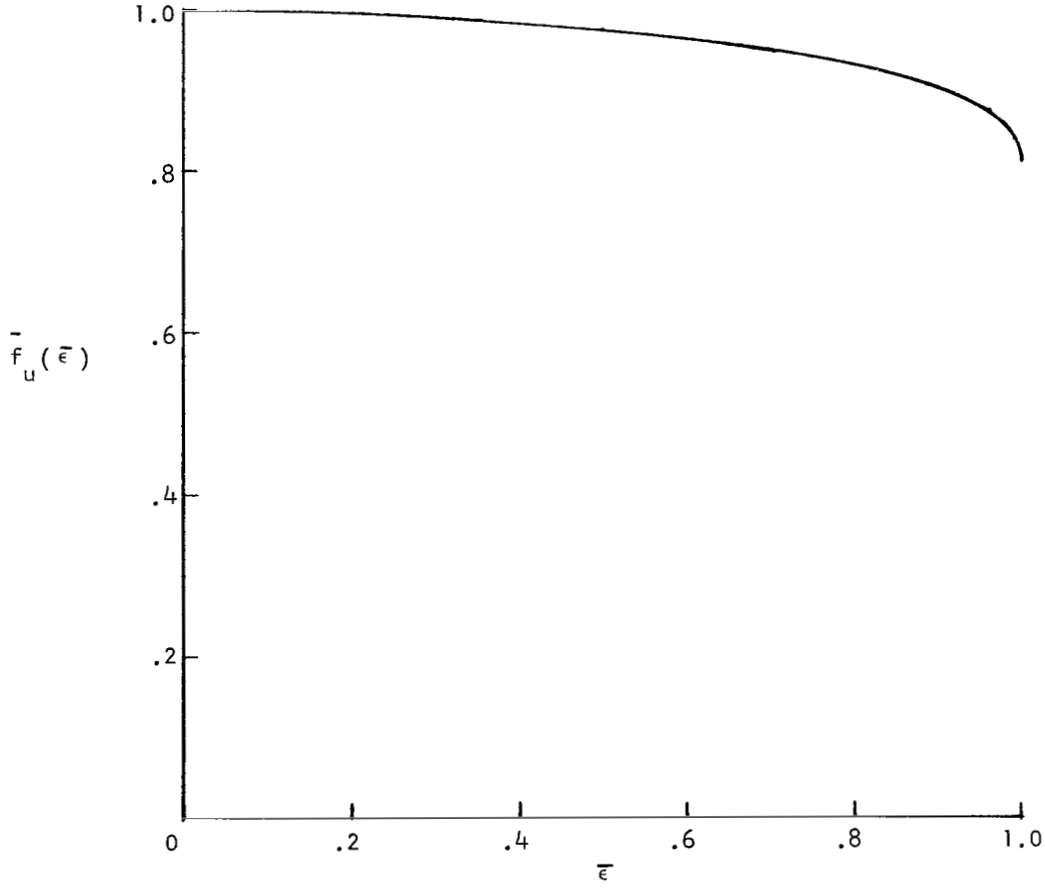

Figure 12.- Variation of function $\bar{f}_u(\bar{\epsilon})$ governing upper bound of time step $\Delta\tau$ with normalized damping coefficient $\bar{\epsilon}$.

010 001 C1 U 12 710723 S00903DS
DEPT OF THE AIR FORCE
WEAPONS LABORATORY /WLOL/
ATTN: E LOU BOWMAN, CHIEF TECH LIBRARY
KIRTLAND AFB NM 87117

"The aeronautical and space activities of the United States shall be conducted so as to contribute . . . to the expansion of human knowledge of phenomena in the atmosphere and space. The Administration shall provide for the widest practicable and appropriate dissemination of information concerning its activities and the results thereof."

—NATIONAL AERONAUTICS AND SPACE ACT OF 1958

NASA SCIENTIFIC AND TECHNICAL PUBLICATIONS

TECHNICAL REPORTS: Scientific and technical information considered important, complete, and a lasting contribution to existing knowledge.

TECHNICAL NOTES: Information less broad in scope but nevertheless of importance as a contribution to existing knowledge.

TECHNICAL MEMORANDUMS: Information receiving limited distribution because of preliminary data, security classification, or other reasons.

CONTRACTOR REPORTS: Scientific and technical information generated under a NASA contract or grant and considered an important contribution to existing knowledge.

TECHNICAL TRANSLATIONS: Information published in a foreign language considered to merit NASA distribution in English.

SPECIAL PUBLICATIONS: Information derived from or of value to NASA activities. Publications include conference proceedings, monographs, data compilations, handbooks, sourcebooks, and special bibliographies.

TECHNOLOGY UTILIZATION PUBLICATIONS: Information on technology used by NASA that may be of particular interest in commercial and other non-aerospace applications. Publications include Tech Briefs, Technology Utilization Reports and Technology Surveys.

Details on the availability of these publications may be obtained from:

SCIENTIFIC AND TECHNICAL INFORMATION OFFICE

NATIONAL AERONAUTICS AND SPACE ADMINISTRATION

Washington, D.C. 20546